

國立交通大學

電信工程研究所

碩士論文

平面式寬頻魔術 T 之設計與合成

Design and Synthesis of Broadband Planar  
Magic-T

研究生：林佩潔

指導教授：張志揚 博士

中華民國 九十九 年 七 月



# 平面式寬頻魔術 T 之設計與合成

## Design and Synthesis of Broadband Planar Magic-T

研究生：林佩潔

Student : Pei-Chieh Lin

指導教授：張志揚 博士

Advisor : Dr. Chi-Yang Chang



A Thesis

Submitted to Institute of Communication Engineering

College of Electrical and Computer Engineering

National Chiao Tung University

In Partial Fulfillment of the Requirements

For the Degree of Master of Science

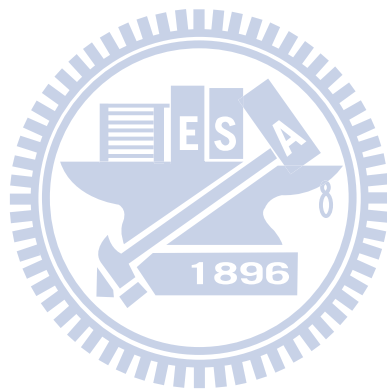
in

Communication Engineering

July 2010

Hsinchu, Taiwan, Republic of China

中華民國 九十九 年 七 月



# 平面式寬頻魔術 T 之設計與合成


研究生：林颯潔

指導教授：張志揚 博士

國立交通大學電信工程研究所

碩士論文

摘要



本論文提出一個新的結構，來實現寬頻的魔術 T。分析上先藉由理查轉換，推導出魔術 T 之電路模型在理查頻域上的等效電路，並將高通原型濾波器的合成法應用於分析此結構上，根據這個方法，設計者得以根據自訂的規格，快速並精確合成出整個魔術 T。



# Design and Synthesis of Broadband Planar Magic-T

Student: Pei-Chieh Lin

Advisor: Dr. Chi-Yang Chang

Institute of Communication Engineering

National Chiao Tung University

## Abstract

A new broadband planar magic-T is presented. By Richard's transformation, we can derive the equivalent circuit model of the magic-T in Richards' domain. Then a synthesis method of the high-pass prototype network will be applied to our circuit model. The magic-T can then be exactly synthesized quickly according to the user-defined specifications such as return loss, bandwidth and impedance transformation ratio.





# Acknowledgement

## 誌 謝

本篇論文得以順利完成，首先要感謝的是我的指導教授張志揚博士。從大學部專題開始就蒙教授指導，讓我一點一滴地累積微波領域的知識和經驗，教授總是樂於和我們分享學業上和生活中的經驗，在研究過程中也給予我們很大的自由，讓我得以依自己的想法去做各種嘗試，並在我遭遇困難時適時給予指導，因此對於這兩年能在教授的指導下完成碩士論文，我感到很幸運。此外，我要特別感謝實驗室學長哲慶、益廷、正憲、忠傑，在研究過程中提供了許多寶貴的建議，以及好友子嫻在實作和量測方面的大力協助，讓我的研究能夠順利完成。

在 916 實驗室的兩年生活是輕鬆而愉快的，不管是尾牙、實驗室聚餐、一同出遊騎腳踏車、謝師宴……對我而言都是十分難忘的回憶。坐鎮於元老區的梁八、Weiga、郭伯總是能幫大家解決各種研究上的疑難雜症；老耿、廖董、Holy、達叔、Jerry，很高興有你們與我一同併肩作戰，一起為了報告煩惱，為了進度打拼；而後加入的新成員：維欣、小水、大蘋果、小鵬，更是為實驗室帶來不少活力。

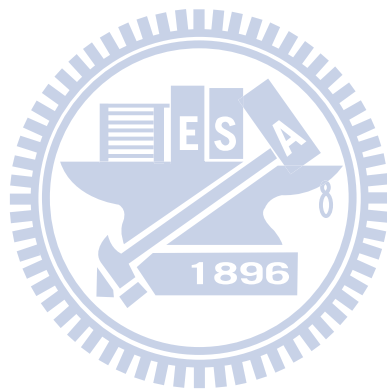
另外不能不提的是，打從大學部就結識至今的好友阿嬪、泡泡、及 Yuna 夫婦，當然還有自大一就結下不解之緣的室友楊紫瓊，無論是課業上還是生活中，都深受你們的幫助，讓我成長不少。回想在交大的這六年，大家也共同營造了許多回憶，一次次的生日聚會、系上營隊、甚至是出國留學時的送機，很開心是你們陪在我身旁。期許在我們脫離學生身分後，都能在各自的領域繼續努力、彼此勉勵，有空再一起出來吃個飯，當然喜帖可少不了我一份囉！

最後，我要感謝默默在背後支持我的家人們，因為有你們的關懷與鼓勵，才能讓我能無後顧之憂地致力於我的學業，真的很感謝你們一直以來的照顧！在此謹以本篇論文表達我的感謝之意。



# Table of Contents

Abstract(Chinese) .....	i
Abstract .....	iii
Acknowledgement .....	v
Table of Contents .....	vii
List of Figures .....	ix
List of Tables.....	xi
Chapter 1 Introduction .....	1
Chapter 2 Basic Theory .....	5
2.1 Introduction.....	5
2.2 Richards' Transformation.....	5
2.3 Kuroda's Identities .....	8
2.4 Element Extraction.....	9
2.4.1 Richards' Theorem.....	9
2.4.2 Pole Removing Techniques.....	10
Chapter 3 The Proposed Broadband Planar Magic-T .....	13
3.1 Introduction.....	13
3.1.1 Full Circuit Model.....	15
3.1.2 Synthesis Procedure .....	17
3.2 Balun Synthesis.....	17
3.3 Power Divider Synthesis.....	23
3.4 Magic-T Transformer.....	28
3.5 Simulation and Implementation .....	31
Chapter 4 Conclusions and Future Works.....	41
References.....	43



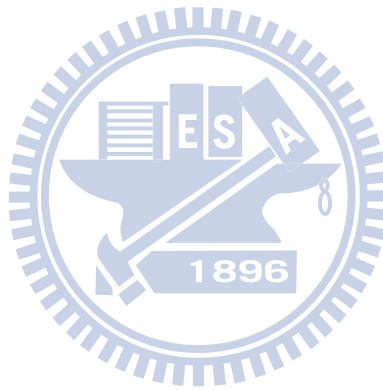
# List of Figures

Figure 1.1 A conventional rat-race ring. ....	1
Figure 1.2 The frequency responses of return loss and insertion loss of the conventional rat-race ring.....	2
Figure 2.1 Mapping properties of the Richard’s Transformation $\frac{S}{j} = \tan \frac{\pi f}{2f_0}$ . (a) Prototype lumped element high-pass. (b) Corresponding distributed element band-pass. ....	6
Figure 3.1 Conceptual block diagram of the proposed broadband magic-T.....	14
Figure 3.2 Full circuit model of the broadband magic-T.....	15
Figure 3.3 Equivalent circuit of the broadband magic-T (in odd mode). ....	16
Figure 3.4 Equivalent circuit of the broadband magic-T (in even mode).....	17
Figure 3.5 Two port network derived from the balun circuit in Figure 3.3. ....	18
Figure 3.6 Balun circuit in high-pass lumped prototype form: (a)Original circuit corresponding to Figure 3.4. (b) Application of the Kuroda’s Identity to $L_1$ and $Z_2$ . (c) Absorbing the transformer by scaling the values of components at the right side of the transformer. (d) Applying the Kuroda’s Identity to $\frac{L_2}{n^2}$ and $\frac{Z_3}{n^2}$ . (e) Absorbing the transformer again. (f) The cascade of shunt inductors are combined to obtain the non-redundant network.....	19
Figure 3.7 Two port high-pass filter prototype of balun.....	20
Figure 3.8 Frequency response of the synthesized balun. ....	23
Figure 3.9 Two port network derived from the divider circuit in Figure 3.3.....	24
Figure 3.10 Power divider circuit in high-pass lumped prototype form: (a) Original circuit corresponding to Figure 3.8. (b) Application of the Kuroda’s Identity to $L_3$ and $Z_5$ . (c) Absorbing the transformer by scaling values of	

components at the right side of the transformer. (d) The cascade of shunt inductors are combined to obtain the non-redundant network. ....	25
Figure 3.11 Two port high-pass filter prototype of the power divider. ....	25
Figure 3.12 Frequency response of the synthesized power divider .....	28
Figure 3.13 Design graph for determining the impedance of common element with specified return loss at (a)50 Ohm, (b) 25 Ohm, and (c) 75 Ohm system. .	31
Figure 3.14 Schematic layout of the fabricated broadband magic-T. ....	33
Figure 3.15 The layouts show (a) the top and (b) the bottom layer of the proposed broadband magic-T.....	34
Figure 3.16 The photographs show (a) the top and (b) the bottom layer of the proposed broadband magic-T.....	35
Figure 3.17 The simulated and measured (a) return loss and (b) insertion loss of the magic-T (in odd mode).....	36
Figure 3.18 The simulated and measured (a) return loss and (b) insertion loss of the magic-T (in even mode). ....	37
Figure 3.19 The simulated and measured isolation at port 2-3 and port 1-4 of the magic-T .....	38
Figure 3.20 The simulated and measured (a) amplitude imbalance and (b) phase imbalance of the magic-T. ....	39

# List of Tables

Table 2.1 ABCD matrix for high-pass elements and corresponding distributed form...	8
Table 2.2 Kuroda's identities .....	9
Table 2.3 Element extraction test and value .....	11
Table 3.1 Theoretical circuit parameters of magic-T. ( $f_o = 2GHz$ ).....	32
Table 3.2 The Physical dimensions of the proposed broadband magic-T corresponding to Figure 3.14. (in mil) .....	33







# Chapter 1

## Introduction

A Magic-T, or 180-degree hybrid, is a fundamental component in microwave circuit and is widely used in applications such as multipliers, balanced mixers, four-port circulators, power amplifiers, and antenna feed networks. In order to achieve low phase and amplitude imbalance, structures with perfect symmetry such as rings are commonly used to form a magic-T. The following figure shows the simplest case - a conventional 180-degree hybrid ring. It's a four-port network. Port 2-1, 1-3, 3-4 are a quarter wavelength away from each other, and port 2-4 are separated by 270-degree. The rat-race ring has a sum port and a difference port that allow incident signals from port 2 and port 3 to be combined or subtracted with a well-defined relative phase. Also when we excite a signal at sum-port or difference-port, we can get in-phase or out-of-phase at ports 2 and port 3, respectively. There are only two kinds of impedance values showing in the conventional rat-race ring, so it's easy to finish the whole circuit design. The complete analysis and design examples are discussed in [1].

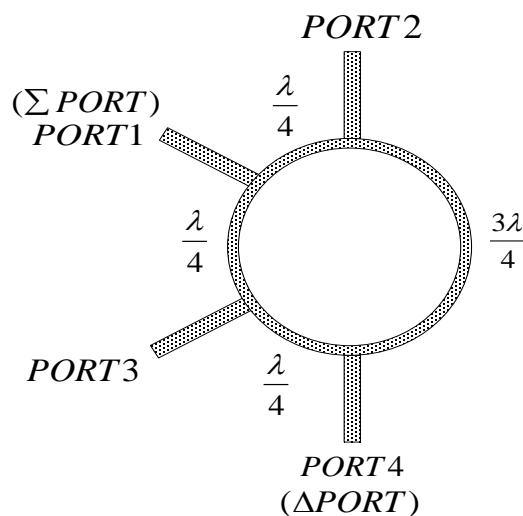


Figure 1.1 A conventional rat-race ring.

The conventional 180 degree hybrid ring contributes a narrow-band frequency response as shown in Figure 1.2, because it only uses limited number of line sections to match all ports.

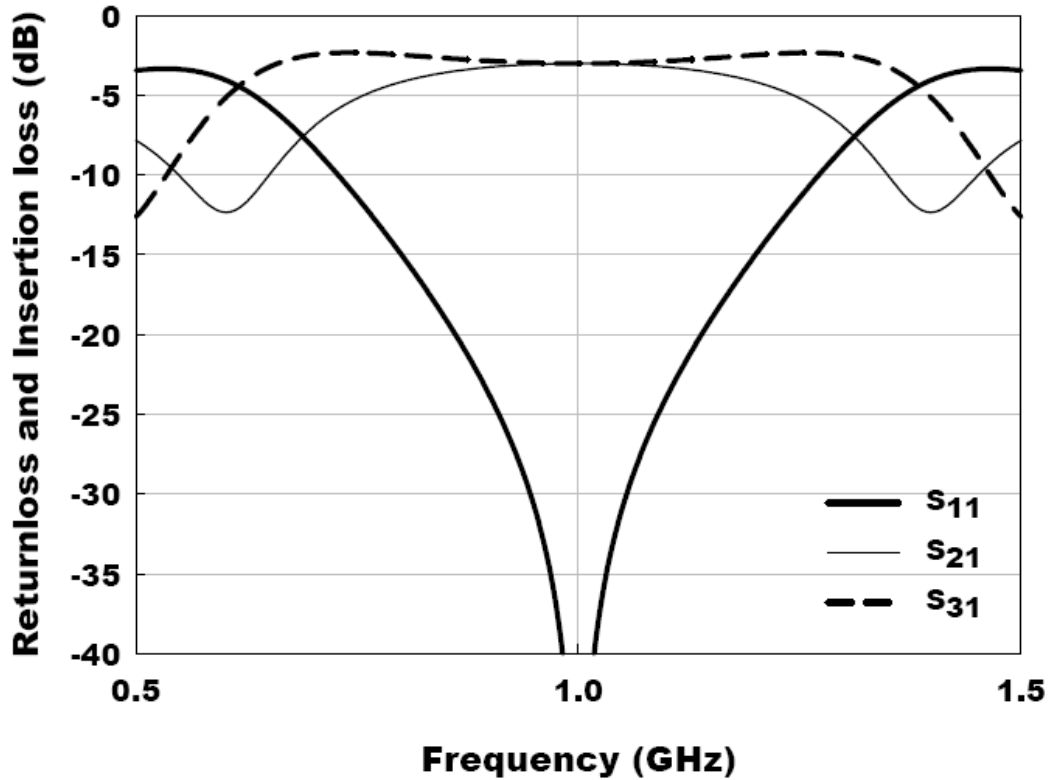
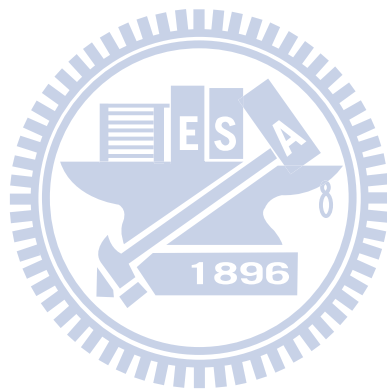


Figure 1.2 The frequency responses of return loss and insertion loss of the conventional rat-race ring

In order to improve the performance of magic-T, several configurations have consequently been developed [2]-[9]. March [2] replaced the  $\frac{3\lambda}{4}$  section of the conventional rat-race ring with a  $\frac{\lambda}{4}$  coupled line. The bandwidth has increased, but the difficulty of implementing the even-mode impedance of the coupled line section using microstrip line structure, which is often used in microwave circuits, limits its use. Considering the demand for compact size circuit, several uniplanar broadband magic-Ts have been proposed [3]-[5]. However, the structures with wire bridges will need further bonding process and thus increase the difficulty of fabrication. To make

the magic-T easy to be fabricated, several double-sided configurations using microstrip -slotline transitions are proposed [6]-[9]. Konhpop U-yen [7]-[9] presents a broadband planar magic-T. It provides more than 70% of 1-dB operating bandwidth about 10GHz, but the equivalent circuit model only approximates the response near the designate frequency. Further optimization process is needed to modify the analytical solution. The technical literatures mentioned above have focused on improving the bandwidth. In many applications, an element with impedance transforming capability is very useful and suitable to be an interface between subsystems with different input and output impedances. K. S. Ang and D. Robertson [10] addressed this problem and demonstrated a planar Marchand balun with output matching function.

In this paper, the proposed broadband planar magic-T, which is based on a high-order Marchand balun, can be fully analyzed and exactly synthesized via the equivalent circuit model we proposed. Impedance-transforming issue is also considered. Some basic theories used in analyzing our structure will be presented briefly in the next chapter. In chapter 3, the proposed magic-T configuration will be investigated thoroughly. First the full circuit model is introduced. Next we illustrate the design and synthesis procedure, and give a complete design example. Some useful design graphs will also be shown. Finally, the simulated and measured results will be discussed.



# Chapter 2

## Basic Theory

### 2.1 Introduction

Network synthesis can be used to find the best approach to a design problem. Once a network is synthesized, it has an optimum result. That is, there is no need to do further optimization to improve the performance. For several decades, methods to exact synthesize a filter with prescribed transfer function has been developed. We are able to apply these synthesis techniques to design low-pass, high-pass, band-pass, and band-stop filters with user-defined electrical performance.

The design of our proposed magic-T is based on the synthesis of a high-pass prototype filter. In this chapter, we first introduce the complex plane transformation that allows us to convert our original distributed network into a lumped prototype network. Then we summarize four Kuroda's Identities which can help us to get the network that is different in form, but is electrically equivalent. Finally, we will focus on the problem of elements extraction if the electrical performance is prescribed.

### 2.2 Richards' Transformation

To accomplish the conversion from a distributed network to a lumped network, Richards proposed a complex plane transformation in 1948. He showed that a distributed network comprised of equal length of transmission-lines and lumped resistors could be treated in analysis or synthesis as lumped R-L-C networks by using the complex variable mapping which is known as Richards' variable. It is defined as

$$S = j\Omega = j \tan \frac{\pi f}{2f_0}, \quad (2.1)$$

where  $\Omega$  is the frequency in Richards domain, and  $f_0$  is the real frequency at which all of the transmission-lines have lengths equal to quarter-wavelength. The mapping properties are demonstrated in Figure 2.1. When we apply the transformation of (2.1) to the high-pass prototype transfer function which has response as shown in Figure 2.1(a), it will exhibit the frequency response repeats in increments of  $2f_0$  due to the periodic nature of the distributed network.

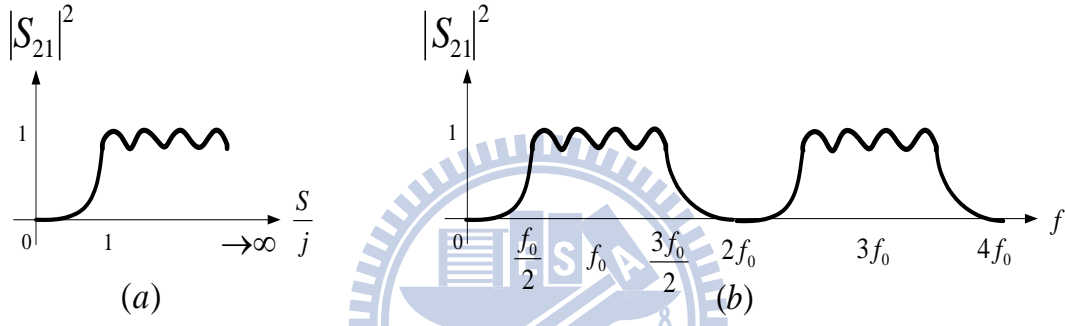


Figure 2.1 Mapping properties of the Richard's Transformation  $\frac{S}{j} = \tan \frac{\pi f}{2f_0}$ .

(a) Prototype lumped element high-pass. (b) Corresponding distributed element band-pass.

In other words, if we want to design a circuit which shows band-pass response in real frequency  $f$  about the quarter-wave frequency  $f_0$ , we can choose high-pass lumped elements as listed in Table 2.1 to form the network and express the whole network as functions of  $S$ .

Horton and Wenzel [11] have provided some appropriate functions for maximally flat ( Butterworth ) and equal ripple ( Chebyshev ) approximation for low-pass and high-pass prototype responses in  $S$ -domain:

$$|S_{21}|^2 = \frac{1}{1 + F_N^2(S)}. \quad (2.2)$$

The maximally flat approximation functions [11] are given by:

$$H.P : F_N^2(S) = \left(\frac{S_C}{S}\right)^{2m} \left(\frac{\sqrt{1-S_C^2}}{\sqrt{1-S^2}}\right)^{2n} = \left(\frac{\tan \theta_C}{\tan \theta}\right)^{2m} \left(\frac{\cos \theta}{\cos \theta_C}\right)^{2n}, \quad (2.3)$$

$$L.P : F_N^2(S) = \left(\frac{S}{S_C}\right)^{2m} \left(\frac{S\sqrt{1-S_C^2}}{S_C\sqrt{1-S^2}}\right)^{2n} = \left(\frac{\tan \theta}{\tan \theta_C}\right)^{2m} \left(\frac{\sin \theta}{\sin \theta_C}\right)^{2n}, \quad (2.4)$$

and the equal ripple approximation functions [11] are given by:

$$\begin{aligned} H.P : F_N^2(S) &= \varepsilon^2 \left[ T_m \left( \frac{S_C}{S} \right) T_n \left( \frac{\sqrt{1-S_C^2}}{\sqrt{1-S^2}} \right) - U_m \left( \frac{S_C}{S} \right) U_n \left( \frac{\sqrt{1-S_C^2}}{\sqrt{1-S^2}} \right) \right]^2 \\ &= \varepsilon^2 \left[ T_m \left( \frac{\tan \theta_C}{\tan \theta} \right) T_n \left( \frac{\cos \theta}{\cos \theta_C} \right) - U_m \left( \frac{\tan \theta_C}{\tan \theta} \right) U_n \left( \frac{\cos \theta}{\cos \theta_C} \right) \right]^2, \end{aligned} \quad (2.5)$$

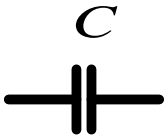
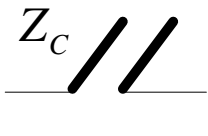

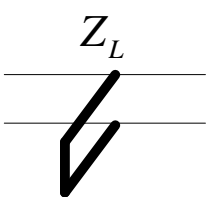
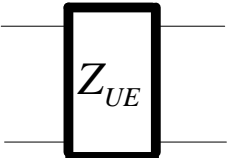

$$\begin{aligned} L.P : F_N^2(S) &= \varepsilon^2 \left[ T_m \left( \frac{S}{S_C} \right) T_n \left( \frac{S\sqrt{1-S_C^2}}{S_C\sqrt{1-S^2}} \right) - U_m \left( \frac{S}{S_C} \right) U_n \left( \frac{S\sqrt{1-S_C^2}}{S_C\sqrt{1-S^2}} \right) \right]^2 \\ &= \varepsilon^2 \left[ T_m \left( \frac{\tan \theta}{\tan \theta_C} \right) T_n \left( \frac{\sin \theta}{\sin \theta_C} \right) - U_m \left( \frac{\tan \theta}{\tan \theta_C} \right) U_n \left( \frac{\sin \theta}{\sin \theta_C} \right) \right]^2, \end{aligned} \quad (2.6)$$

where  $T_m(x) = \cos(m \cos^{-1} x)$  is the Chebyshev polynomial of the first kind and

$U_m(x) = \sin(m \cos^{-1} x)$  is the m-th degree unnormalized Chebyshev polynomial of

the second kind. Once the number of high-pass elements, return loss, and bandwidth are specified, we can derive the transfer function in  $S$ -plane.

Table 2.1 ABCD matrix for high-pass elements and corresponding distributed form

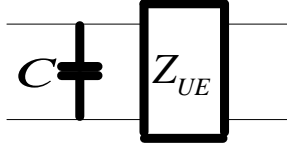
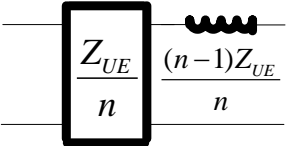
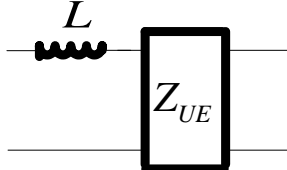
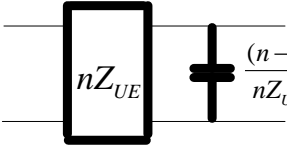
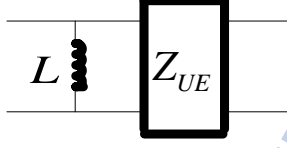
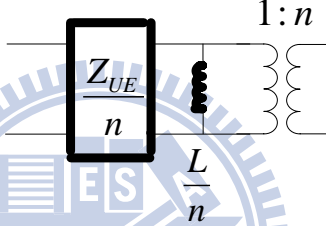
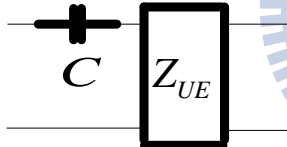
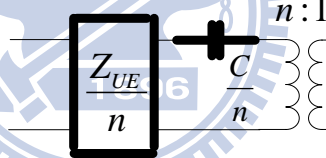
<i>High – pass elements</i>	<i>Distubuted Form</i>	<i>ABCD Matrix</i>
		$\begin{bmatrix} 1 & \frac{1}{SC} \\ 0 & 1 \end{bmatrix}$
		$\begin{bmatrix} 1 & 0 \\ \frac{1}{SL} & 1 \end{bmatrix}$
		$\frac{1}{\sqrt{1-S^2}} \begin{bmatrix} 1 & SZ_{UE} \\ \frac{S}{Z_{UE}} & 1 \end{bmatrix}$

## 2.3 Kuroda's Identities

The following table summarizes the four Kuroda's Identities, and they can be proven to be exactly the same by deriving the ABCD matrix of the original networks and equivalent networks in Table 2.2. The transformations improve the flexibility when we design circuits. Sometimes we need to add redundant elements to obtain a network configuration which is more realizable. Besides, Kuroda's Identities often can be applied to provide the unequal terminations. When introducing sufficient redundancy to transform a non-realizable topology into one that can be implemented, or alter element values to more practical levels, we can always use Kuroda's Identities to obtain the equivalent non-redundant network.



Table 2.2 Kuroda's identities

<i>Original network</i>	<i>Equivalent network</i>	$n$
		$1 + Z_{UE}C$
		$1 + \frac{L}{Z_{UE}}$
		$1 + \frac{Z_{UE}}{L}$
		$1 + \frac{1}{Z_{UE}C}$

## 2.4 Element Extraction

If the  $S$ -plane input impedance of the two-port network can be derived from the specified transfer function, we can apply Richards' theorem to determine the value of the cascaded transmission line, known as an unit element (UE), and pole removing techniques are used to find the LC values.

### 2.4.1 Richards' Theorem

The value of a transmission line element can be determined by Richards' theorem [12]. It states

*“A unit element of characteristic impedance  $Z(1)$  can always be extracted from a positive real rational impedance  $Z(S)$  leaving a remainder of*

$$Z'(S) = Z(1) \frac{Z(S) - SZ(1)}{Z(1) - SZ(S)},$$

*which is also rational and positive real of degree at most equal to that of*

*$Z(S)$ . Furthermore, if  $Ev\{Z(1)\} = 0$ ,*

*i.e., the even component of  $Z(S)$  evaluated at  $S=1$  equals 0, then*

$$\deg\{Z'(S)\} = \deg\{Z(S)\} - 1.”$$





From the descriptions above, we know that if the even component of  $Z(S)$  evaluated at  $S=1$  is 0, the degree of the input impedance function will be reduced by one.  $Z'(S)$  seems to be one degree higher than  $Z(S)$  due to the additional factor of  $S$  in the denominator and numerator. However, they are both rational and 0 for  $S=1$ , so we can eliminate the common term  $(S-1)$  from the denominator and numerator. Likewise, if  $Z(-1) = -Z(1)$ , the denominator and numerator are 0 at  $S= -1$ . Then the common term  $(S+1)$  can be removed, which lowers the degree of  $Z(S)$  to be one less than  $Z(S)$ .

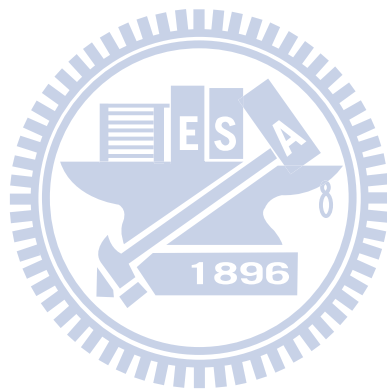
## 2.4.2 Pole Removing Techniques

The element extraction method based on the poles of  $Z(S)$  of  $Y(S)$  is usually used to find LC values [13]-[16]. Table 2.3 shows four ideal lumped elements and their corresponding  $S$ -plane impedance or admittance. We can see the poles of inductors and capacitors occur at  $S = 0$  or  $S \rightarrow \infty$ . For example, if a series capacitor is connected to the input port,  $Z(S)$  will be infinite at  $S = 0$ , and it is independent of the other elements in the network. Then we can manipulate  $Z(S)$  into the sum of the impedance of the capacitor plus the remainder term, and evaluate a value of  $S$  which

eliminates the remainder term and get the value of the capacitor. The following table summarizes the result of determining LC values when the impedance function is given.

Table 2.3 Element extraction test and value

<i>Element</i>	<i>Z(S) or Y(S)</i>	<i>Pole</i>	<i>Value</i>
	$Z(S) = SL$	$Z(S) _{S \rightarrow \infty}$	$L = \frac{p_n}{q_m}$
	$Y(S) = \frac{1}{SL}$	$Y(S) _{S \rightarrow 0}$	$L = \frac{p_1}{q_0}$
	$Z(S) = \frac{1}{SC}$	$Z(S) _{S \rightarrow 0}$	$C = \frac{q_1}{p_0}$
	$Y(S) = SC$	$Y(S) _{S \rightarrow \infty}$	$C = \frac{q_m}{p_n}$
$Z(S) = \frac{P(S)}{Q(S)} = \frac{p_n S^n + \dots + p_2 S^2 + p_1 S + p_0}{q_m S^m + \dots + q_2 S^2 + q_1 S + q_0}$			



# Chapter 3

## The Proposed Broadband Planar Magic-T

### 3.1 Introduction

With the rapid growing of the microwave techniques, the Magic-T is indispensable in applications such as balanced mixers, amplifiers, and frequency discriminators. Over the past years, several structures have been developed to design a magic-T. One commonly used technique is to convert a balun circuit into 180-degree hybrid by appropriately adding an in-phase power divider [17]. The conventional rat-race ring introduced in Chapter 1 only has narrow band response, and we know that using more line sections to match all of the the ports can improve the bandwidth, but it also increases the complexity of the circuit. Hence, there is a demand for a systematical method to analyze and design the circuit especially when the number of the lines increases as the operating bandwidth goes up.

Because of the above problems, we are trying to find an exact synthesis method to design the magic-T. Unlike the conventional try-and-error process, once the synthesis is completed, there is no need to do any optimization and thus save much time. A well established synthesis technique for filter design is applied to our structure. By taking advantage of the method of filter design, we can expect to synthesize the magic-T according to prescribed specifications such as bandwidth, pass band return loss and the impedance of output ports. Besides, the equivalent circuit model of the magic-T will be manipulated by Richards' Transformation and Kuroda's Identities. Since the equivalences of the transformation apply at all frequencies, our circuit model can describe the performance in pass band pretty well.

In this chapter, a novel broadband planar magic-T, which is based on the equivalent circuit of a Marchand balun, will be presented. We design an in-phase power divider which can incorporate with the balun circuit via a common element. To achieve a wide bandwidth property, the balun and the power divider are both designed to exhibit fifth-order response. The conceptual block diagram is shown in Figure 3.1. In the following sections, the full circuit model of the magic-T will be presented first and then simplified for odd and even mode cases, respectively. Richrads' transform and Kuroda's identities are applied to simplify the circuit into a non-redundant two port network form. Then, an exact synthesis based on the design of filter prototypes can be used to determine all of the element values. Finally, the key point to design the magic-T with impedance-transforming function will be discussed and some graphs are presented to provide us with an insight into our design problem.

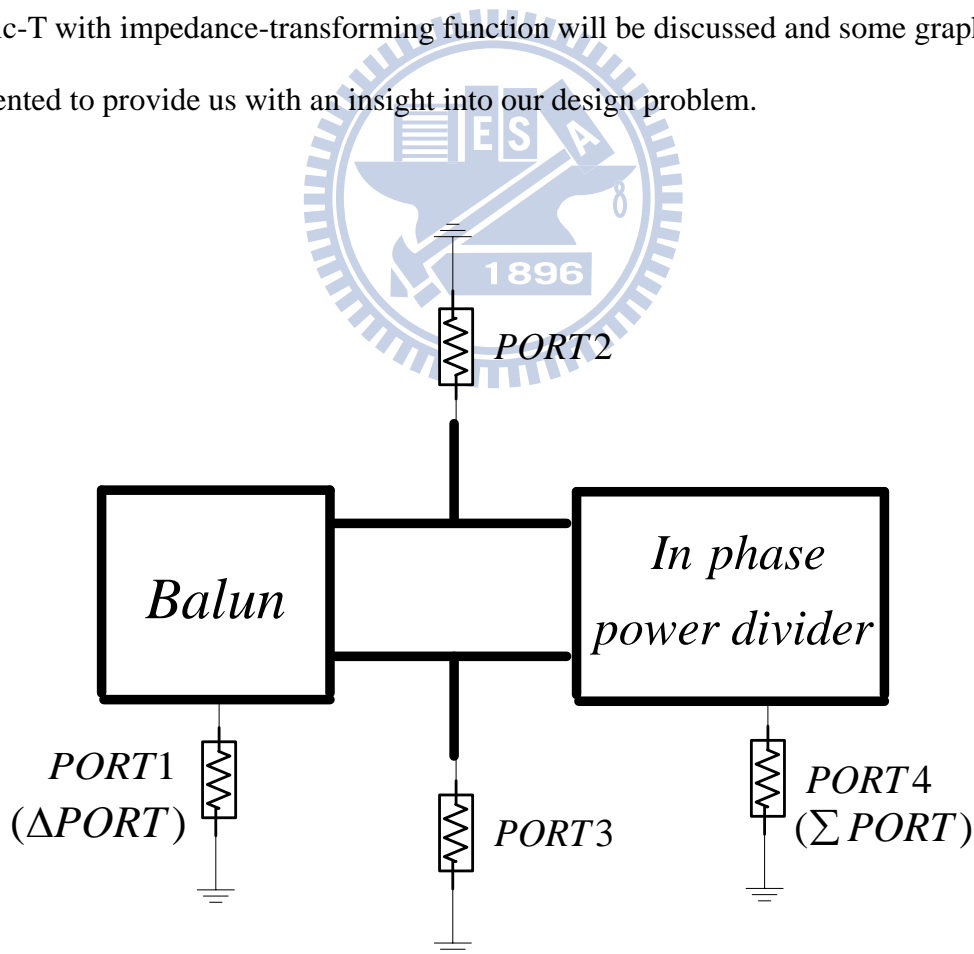


Figure 3.1 Conceptual block diagram of the proposed broadband magic-T.

### 3.1.1 Full Circuit Model

The full circuit model of the proposed magic-T, as shown in Figure 3.2, can be divided into two sections. The left part is a fifth-order Marchand balun, and the right part is a fifth-order power divider. The whole network consists of commensurate length lines. Namely, all of the transmission-lines and stubs are set to be quarter-wavelength at designate frequency.

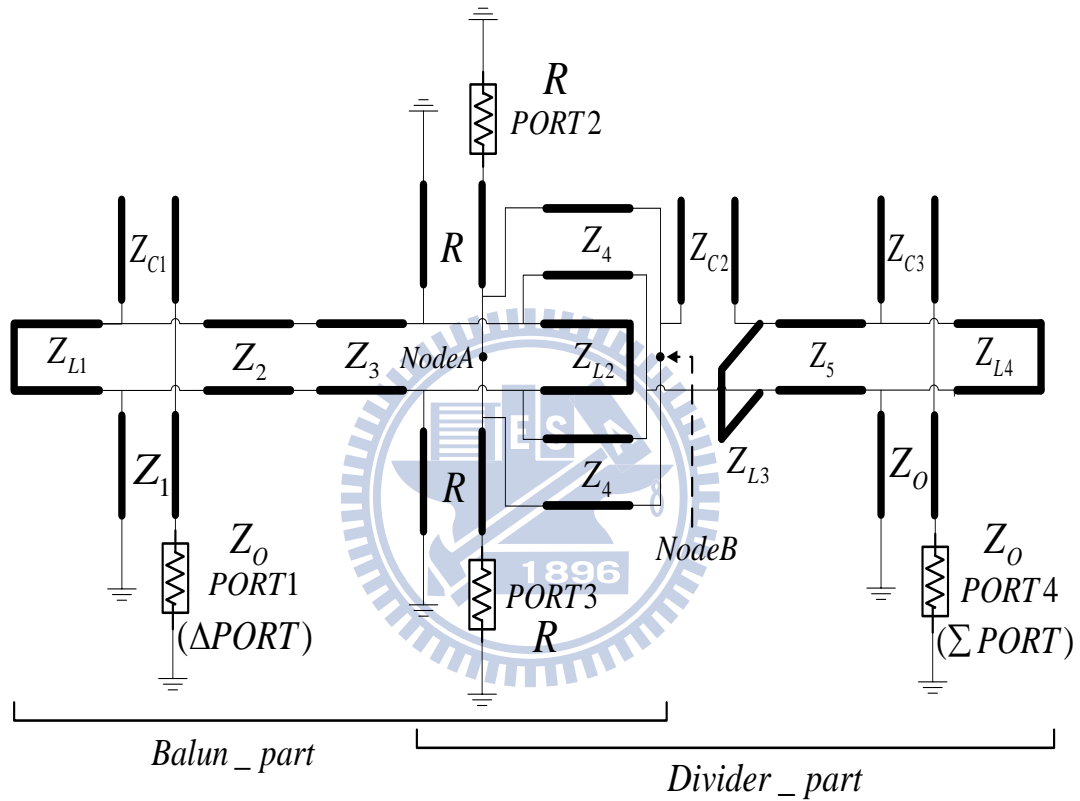


Figure 3.2 Full circuit model of the broadband magic-T.

The magic-T can be analyzed in both odd and even modes. We'll get two equivalent circuits under two modes. When signal is excited at port 1 (difference port), the magic-T is in the odd mode and the signals at port2 and port3 are out-of-phase, thus creating a virtual ground at node B, as shown in the figure 3.2. Likewise, in even mode, the signal is excited at sum port and we'll get in-phase outputs at port 2 and

port 3, and this will create a virtual open at node A. The equivalent circuits of the magic-T under two modes are shown in Figure 3.3 and Figure 3.4.

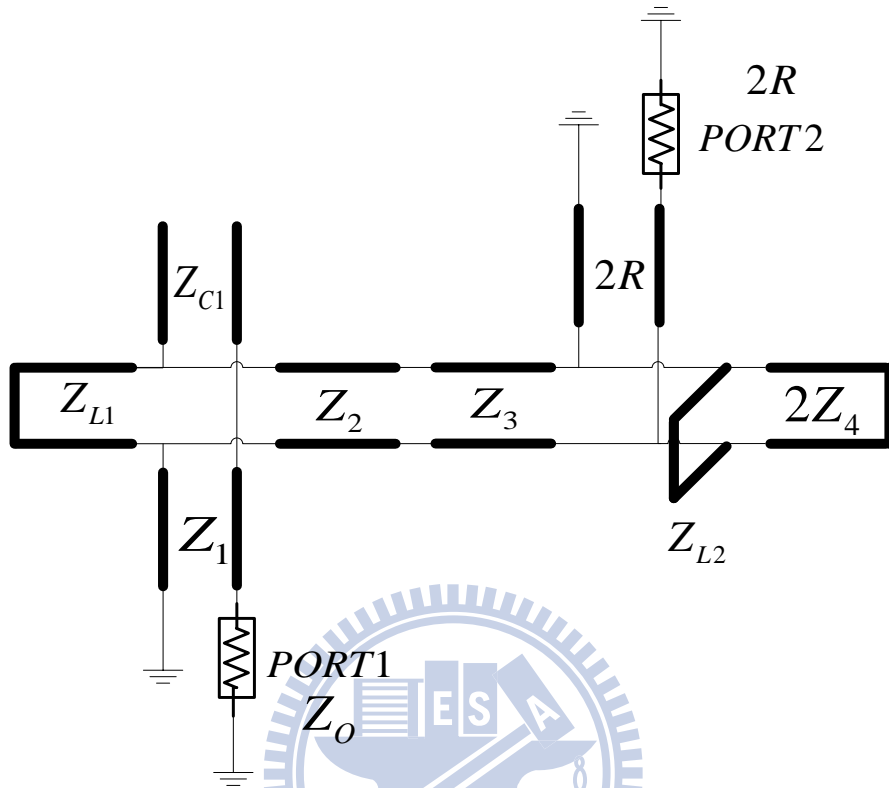


Figure 3.3 Equivalent circuit of the broadband magic-T (in odd mode).

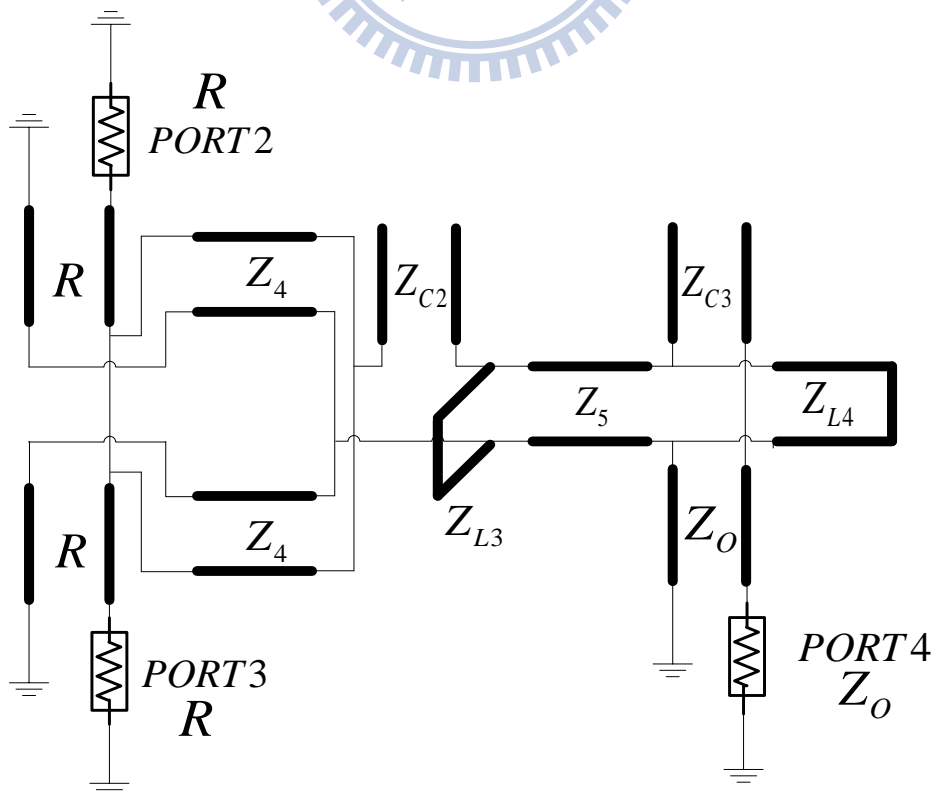




Figure 3.4 Equivalent circuit of the broadband magic-T (in even mode).

### 3.1.2 Synthesis Procedure

The synthesis procedure of the magic-T network includes the following steps:

- (1) Transform the original distributed network composed of entirely quarter-wavelength lines into two-port lumped network by performing Richards' Transformation given in (2.1).
- (2) Apply Kuroda's identities to obtain a cascade of UE and lumped elements that forming a non-redundant network.
- (3) Determine the appropriate approximation function that exhibits desired response in pass band. Two most commonly used approximations, Butterworth and Chebyshev approximations for low-pass and high-pass prototype results in  $S$ -domain are given in Chapter 2. In our design case, we'll choose equal ripple approximation given in (2.5) as our synthesis target.
- (4) Derive the input impedance function of  $S$ -plane from the approximation function and then use Richards' theorem and pole removing techniques to extract element values.
- (5) The extracted element values of  $L$ ,  $C$ , and UE then can be de-normalized to evaluate the impedance for each line section of the original distributed network.

## 3.2 Balun Synthesis

When signal is excited at difference port, we'll get out-of-phase signals at port 2 and port 3. The magic-T now works as a balun and its equivalent circuit is shown in Figure 3.3, and the two port network form, which is shown in Figure 3.5, can be

obtained by combining port2 and port 3 in series connection. Then Kuroda's identities are applied to simplify the circuit into a non-redundant two-port network, which is used in our synthesis. The simplification process is shown in Figure 3.6 (a) to (f).

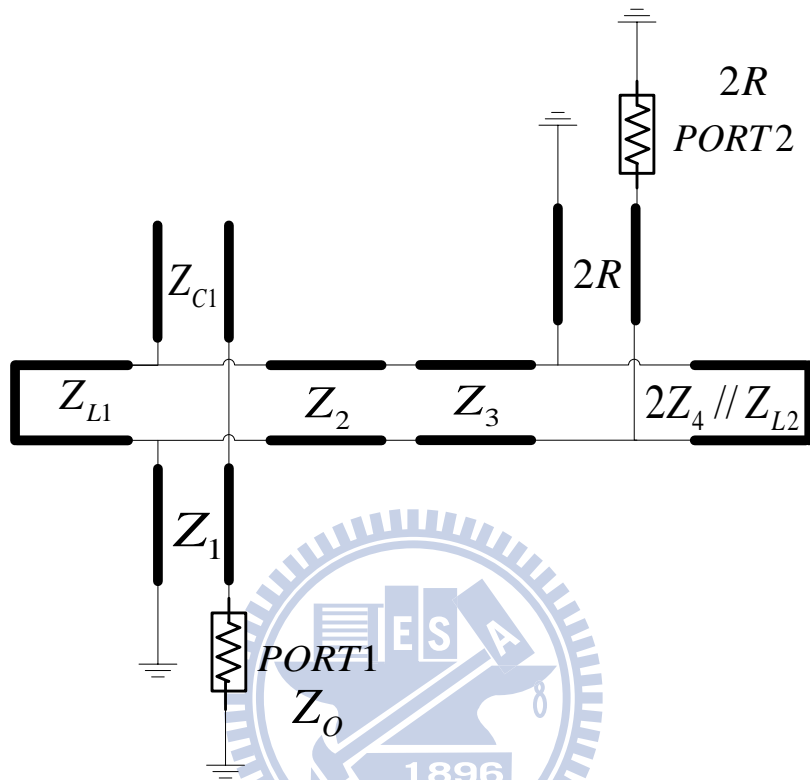
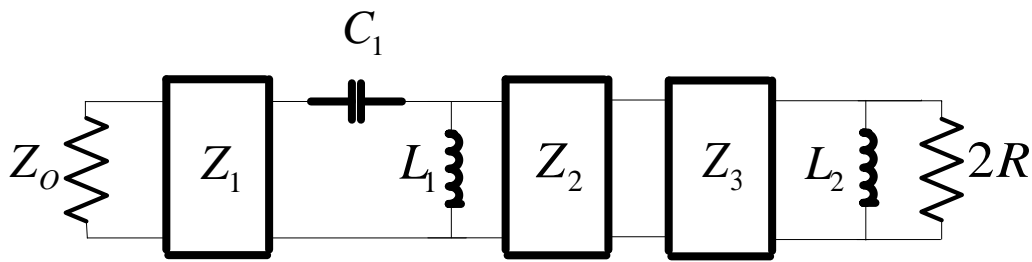
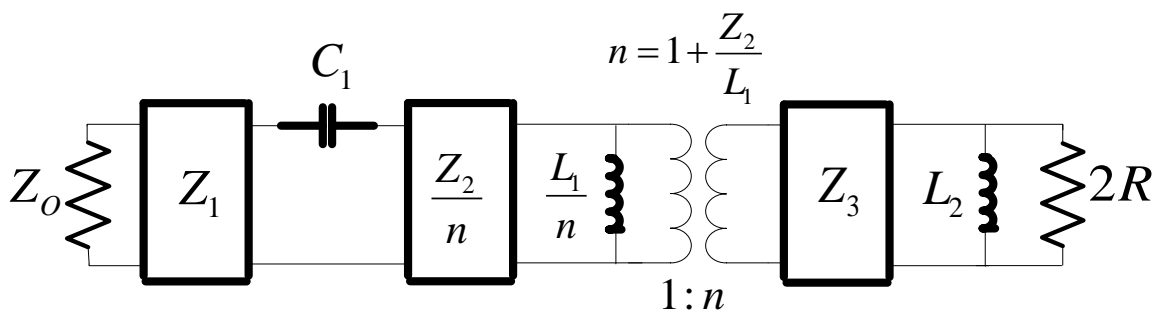


Figure 3.5 Two port network derived from the balun circuit in Figure 3.3.



(a)



(b)

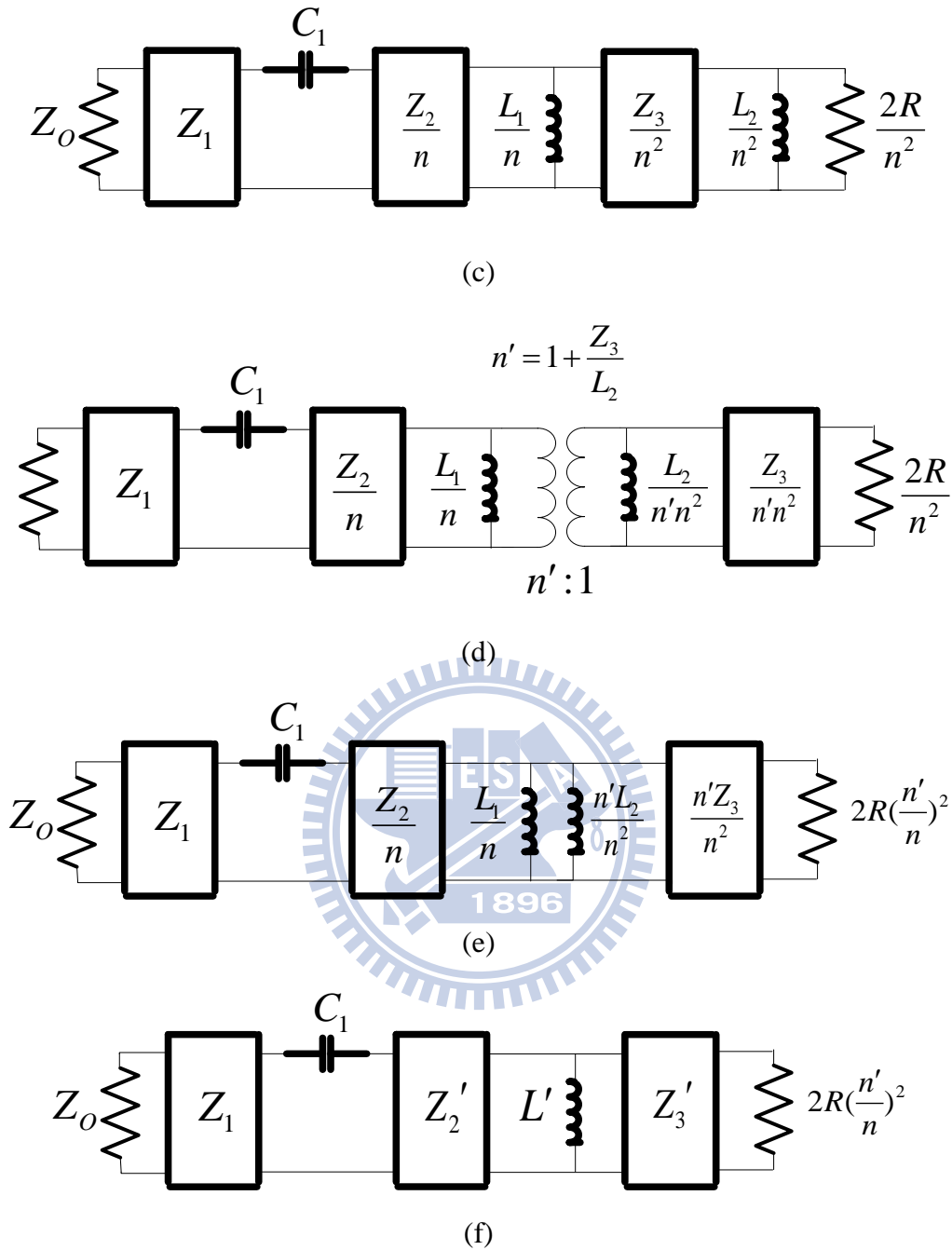


Figure 3.6 Balun circuit in high-pass lumped prototype form: (a)Original circuit corresponding to Figure 3.4. (b) Application of the Kuroda's Identity to  $L_1$  and  $Z_2$ . (c) Absorbing the transformer by scaling the values of components at the right side of the transformer. (d) Applying the Kuroda's Identity to  $\frac{L_2}{n^2}$  and  $\frac{Z_3}{n^2}$ . (e) Absorbing the transformer again. (f) The cascade of shunt inductors are combined to obtain the non-redundant network.

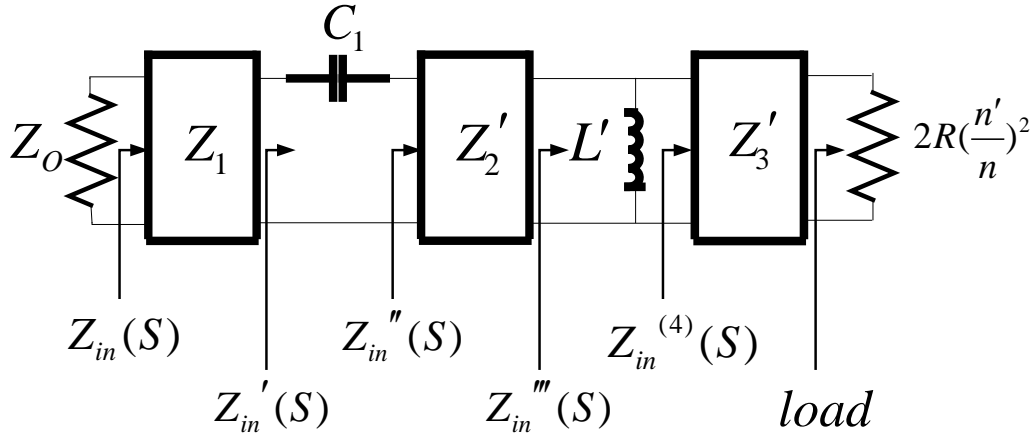


Figure 3.7 Two port high-pass filter prototype of balun.

Now we have a two port high-pass filter prototype as shown in Figure 3.7. In our design example, a fifth-order equal-ripple band-pass filter of 3 to 1 bandwidth will be synthesized. The network composed of three unit elements and two LC elements will be designed to have return loss under -15dB in pass band. The normalized cut off frequency for a 3 to 1 bandwidth is  $S_c = j$ . We substitute all the parameters into (2.5) and get the transfer function below:

$$|S_{21}|^2 = \frac{1}{1 + F_N^2(S)} = \frac{1}{1 + \varepsilon^2 \left[ T_2\left(\frac{S_c}{S}\right) T_3\left(\frac{\sqrt{1-S_c^2}}{\sqrt{1-S^2}}\right) - U_2\left(\frac{S_c}{S}\right) U_3\left(\frac{\sqrt{1-S_c^2}}{\sqrt{1-S^2}}\right) \right]^2}. \quad (3.1)$$

The power conservation gives the relationship:

$$|S_{11}|^2 + |S_{21}|^2 = 1. \quad (3.2)$$

Substitute (3.1) into (3.2) and simplify the polynomials, we have:

$$|S_{11}|^2 = \frac{1.2324S^8 + 12.4591S^6 + 42.6011S^4 + 56.166S^2 + 25.0446}{-S^{10} + 4.2324S^8 + 9.4591S^6 + 43.6011S^4 + 56.166S^2 + 25.0446}. \quad (3.3)$$

The numerator of  $|S_{11}|^2$  is a perfect square, so we can derive the numerator of

$S_{11}$  by inspection. The roots of the denominator can be found using math tool such as MATLAB. We choose the left-hand plane poles to be associated with  $S_{11}$  to form a stable system. The polynomial of the input reflection coefficient is

$$S_{11}(S) = \frac{1.1101S^4 + 5.6116S^2 + 5.0045}{S^5 + 4.9106S^4 + 9.9407S^3 + 12.7456S^2 + 8.4501S + 5.0045} . \quad (3.4)$$

Use the linear transformation:

$$Z_{in}(S) = \frac{1 + S_{11}(S)}{1 - S_{11}(S)} . \quad (3.5)$$

After some arrangement we can obtain the input impedance function of  $S$ :

$$Z_{in}(S) = \frac{S^5 + 6.0207S^4 + 9.9407S^3 + 18.3572S^2 + 10.0089}{S^5 + 3.8005S^4 + 9.9407S^3 + 7.134S^2 + 8.4501S} . \quad (3.6)$$

As illustrated in Figure 3.7, the first element seen from input port is a unit element and Richards' theorem can be applied to give:

$$Z_1 = Z_{in}(1) \approx 1.7734 . \quad (3.7)$$

The input impedance of the remainder network after removing  $Z_1$  is:

$$Z_{in}'(S) = Z_{in}(1) \frac{SZ_{in}(1) - Z_{in}(S)}{SZ_{in}(S) - Z_{in}(1)} ,$$

or

$$Z_{in}'(S) = \frac{3.1448S^4 + 10.1783S^3 + 23.7295S^2 + 14.985S + 17.7494}{S^4 + 4.2473S^3 + 4.2011S^2 + 4.9761S} , \quad (3.8)$$

after cancelling of the common  $S^2 - 1$  factor.

Next, the value of a series capacitor  $C_1$  is determined by pole removing method.

$$C_1 = \frac{4.9761}{17.7494} \approx 0.2804 . \quad (3.9)$$

After removing the series capacitor, the input impedance of the network becomes

$$Z_{in}''(S) = \frac{3.1448S^4 + 6.6114S^3 + 8.5796S^2}{S^4 + 4.2473S^3 + 4.2011S^2 + 4.9761S} . \quad (3.10)$$

Richards' theorem is applied again to get  $Z_2'$  and  $Z_{in}'''(S)$ .

$$Z_2' = Z_{in}''(1) \approx 1.2712 , \quad (3.11)$$

$$Z_{in}'''(S) = \frac{0.5138S^3 + 0.9112S^2}{S^3 + 1.6981S^2 + 2.0114S} . \quad (3.12)$$

The shunt inductor of value of  $L'$  and the final unit element  $Z_3'$  are removed in a similar manner:

$$L' = \frac{0.9112}{2.0114} \approx 0.453 , \quad (3.13)$$

$$Z_{in}^{(4)}(S) = \frac{0.5138S^3 + 0.9112S^2}{S^3 + 0.5639S^2} , \quad (3.14)$$

$$Z_3' = Z_{in}^{(4)}(1) \approx 0.9112 . \quad (3.15)$$

The value of the termination with scaling factor  $(\frac{n'}{n})^2$  is:

$$Load \approx 1.6158 . \quad (3.16)$$

Now all of the element values are obtained and can be de-normalized to evaluate the impedance of the transmission lines. The frequency for which the transmission

lines are a quarter-wavelength is set to be 2GHz. Figure 3.8 shows the frequency response of the synthesized balun.

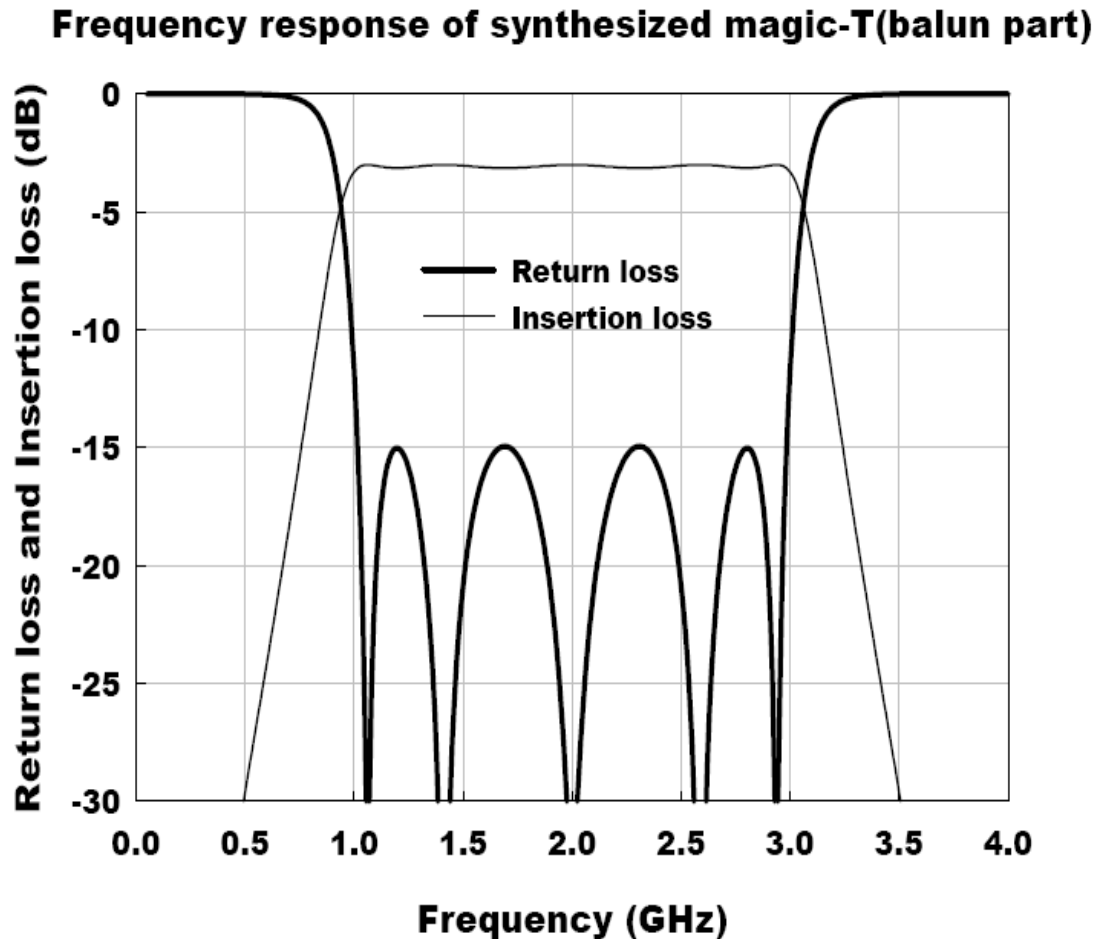


Figure 3.8 Frequency response of the synthesized balun.

### 3.3 Power Divider Synthesis

The synthesis procedure has no difference between balun and divider circuit. Figure 3.9 shows the two port network obtained by parallel port2 with port 3 in Figure 3.4. Kuroda's identities are still needed to simplify the circuit into a non-redundant two-port network. The simplification process is shown in Figure 3.10 (a) to (d).

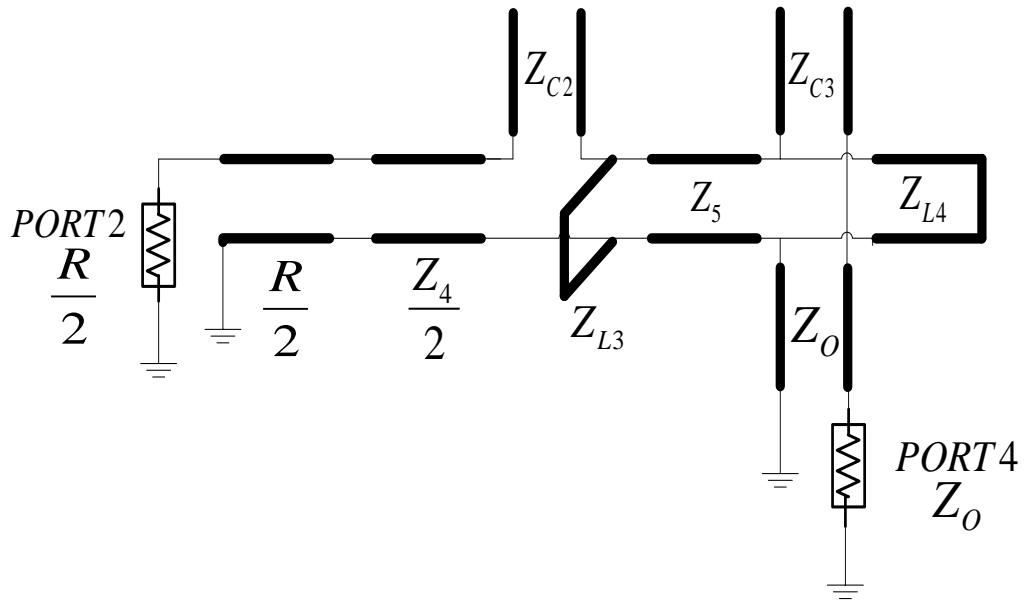
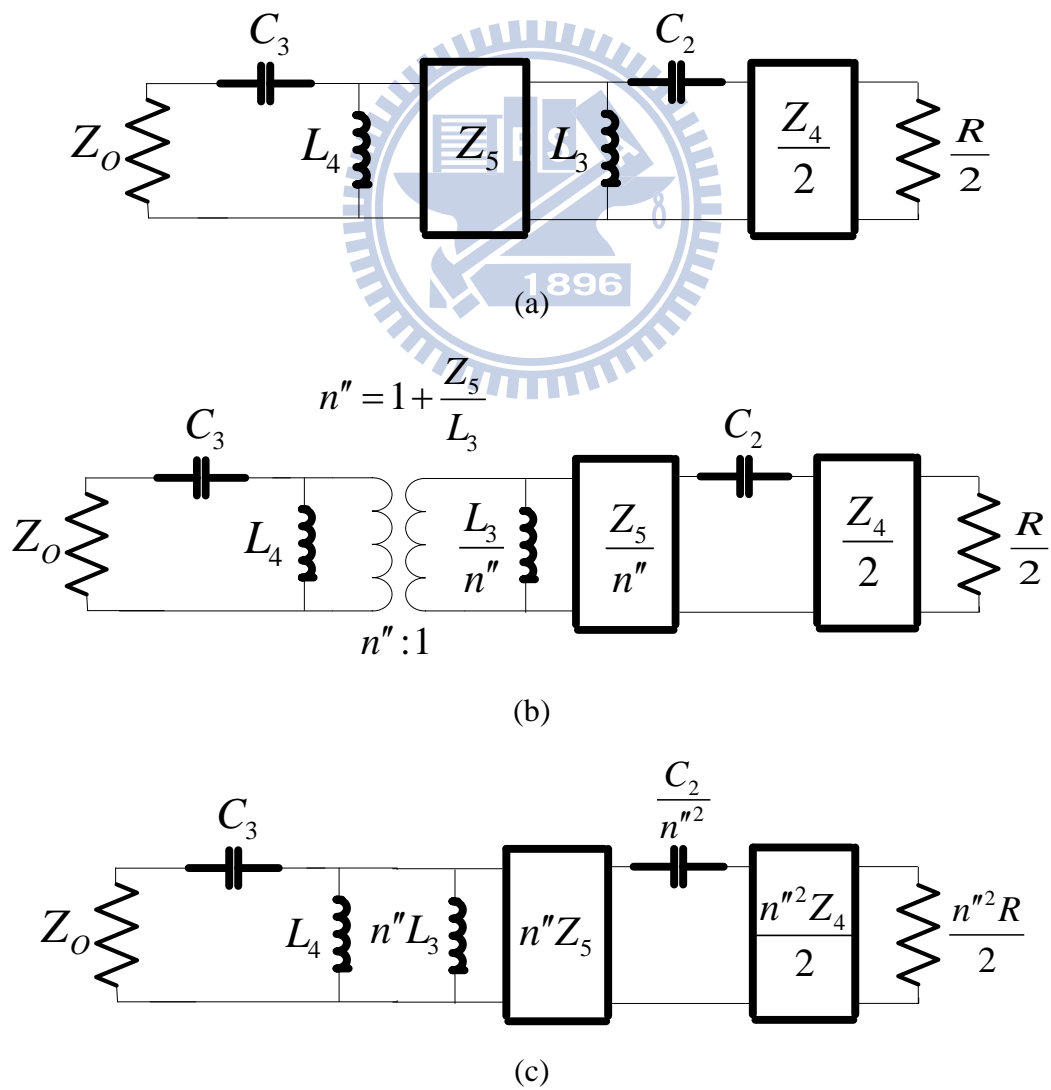
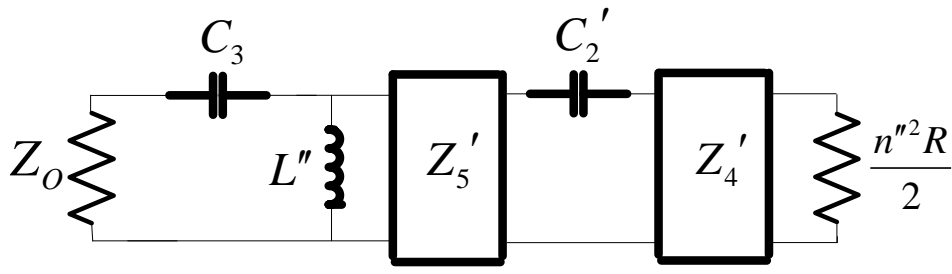


Figure 3.9 Two port network derived from the divider circuit in Figure 3.3.







(d)

Figure 3.10 Power divider circuit in high-pass lumped prototype form: (a) Original circuit corresponding to Figure 3.8. (b) Application of the Kuroda's Identity to  $L_3$  and  $Z_5$ . (c) Absorbing the transformer by scaling values of components at the right side of the transformer. (d) The cascade of shunt inductors are combined to obtain the non-redundant network.

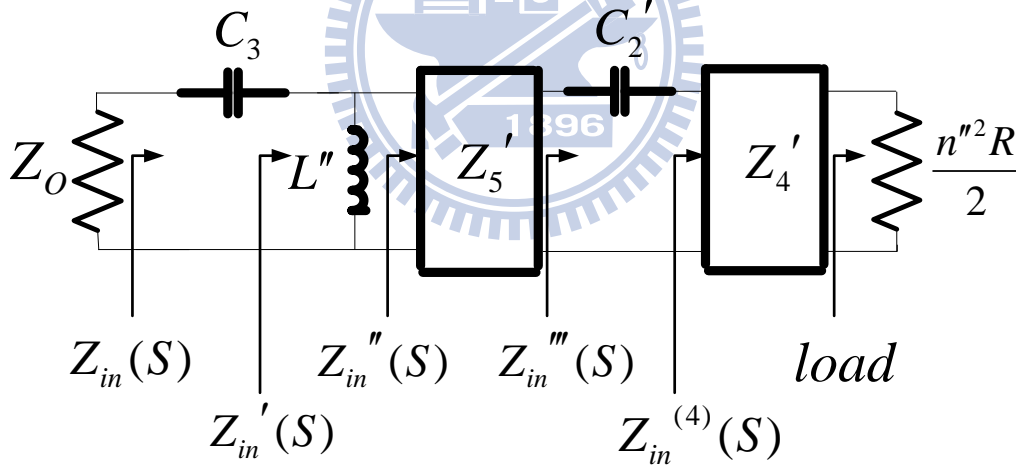


Figure 3.11 Two port high-pass filter prototype of the power divider.

Figure 3.11 is the two port high-pass filter prototype of the divider circuit. Again we choose to synthesize a fifth-order equal-ripple band-pass filter of 3 to 1 bandwidth. The network, consisting of two unit elements and three LC elements, will be designed to have return loss under -15dB in pass band. After substituting parameters into (2.5) we get the transfer function:

$$|S_{21}|^2 = \frac{1}{1 + F_N^2(S)} = \frac{1}{1 + \varepsilon^2 \left[ T_3 \left( \frac{S_c}{S} \right) T_2 \left( \frac{\sqrt{1-S_c^2}}{\sqrt{1-S^2}} \right) - U_3 \left( \frac{S_c}{S} \right) U_2 \left( \frac{\sqrt{1-S_c^2}}{\sqrt{1-S^2}} \right) \right]^2}. \quad (3.17)$$

We manipulate the polynomials in a similar manner to obtain the input impedance function of  $S$ :

$$|S_{11}|^2 = \frac{1.0742S^8 + 10.0052S^6 + 31.8903S^4 + 40.0208S^2 + 17.1879}{-S^{10} + 3.0742S^8 + 9.0052S^6 + 31.8903S^4 + 40.0208S^2 + 17.1879}, \quad (3.18)$$

$$S_{11}(S) = \frac{1.0365S^4 + 4.8266S^2 + 4.1458}{S^5 + 4.4741S^4 + 8.4719S^3 + 10.5697S^2 + 6.9006S + 4.1458}, \quad (3.19)$$

$$Z_{in}(S) = \frac{S^5 + 5.5106S^4 + 8.4718S^3 + 15.396S^2 + 6.9005S + 8.2917}{S^5 + 3.4377S^4 + 8.4718S^3 + 5.7427S^2 + 6.9005S}. \quad (3.20)$$

The first element to be removed is a series capacitor. Its value and the remainder term are:

$$C_3 = \frac{6.9005}{8.2917} \approx 0.8322, \quad (3.21)$$

$$Z_{in}'(S) = \frac{S^5 + 4.309S^4 + 4.3411S^3 + 5.2162S^2}{S^5 + 3.4377S^4 + 8.4718S^3 + 5.7427S^2 + 6.9005S}. \quad (3.22)$$

Another LC element is extracted by applying pole removing techniques and the impedance of the remainder network is:

$$L'' = \frac{5.2162}{6.9005} \approx 0.7559, \quad (3.23)$$

$$Z_{in}''(S) = \frac{S^5 + 4.309S^4 + 4.3411S^3 + 5.2162S^2}{S^5 + 2.1148S^4 + 2.7715S^3}. \quad (3.24)$$

Applying Richards' theorem to remove the third element and find  $Z_{in}'''(S)$ :

$$Z_5' = Z_{in}''(1) \approx 2.5256, \quad (3.25)$$

$$Z_{in}'''(S) = \frac{6.3786S^4 + 10.9637S^3 + 13.174S^2}{S^4 + 1.7834S^3}. \quad (3.26)$$

Next, a series capacitor of value  $C_2'$  and  $Z_{in}^{(4)}(S)$  are given:

$$C_2' = \frac{1.7834}{13.174} \approx 0.1354, \quad (3.27)$$

$$Z_{in}^{(4)}(S) = \frac{6.3786S^4 + 3.5766S^3}{S^4 + 1.7834S^3}. \quad (3.28)$$

Finally we extract the unit element  $Z_4'$  and the value of the termination.

$$Z_4' = Z_{in}^{(4)}(1) \approx 3.5766, \quad (3.29)$$

$$Load \approx 2.0055. \quad (3.30)$$

All elements of the divider are determined and the response is shown in Figure 3.12. The performance of synthesized balun and divider both shows perfect match with the transfer function we prescribed. In the next part we'll further complete the synthesis of the whole magic-T and show how to design an impedance-transforming 180 degree hybrid.

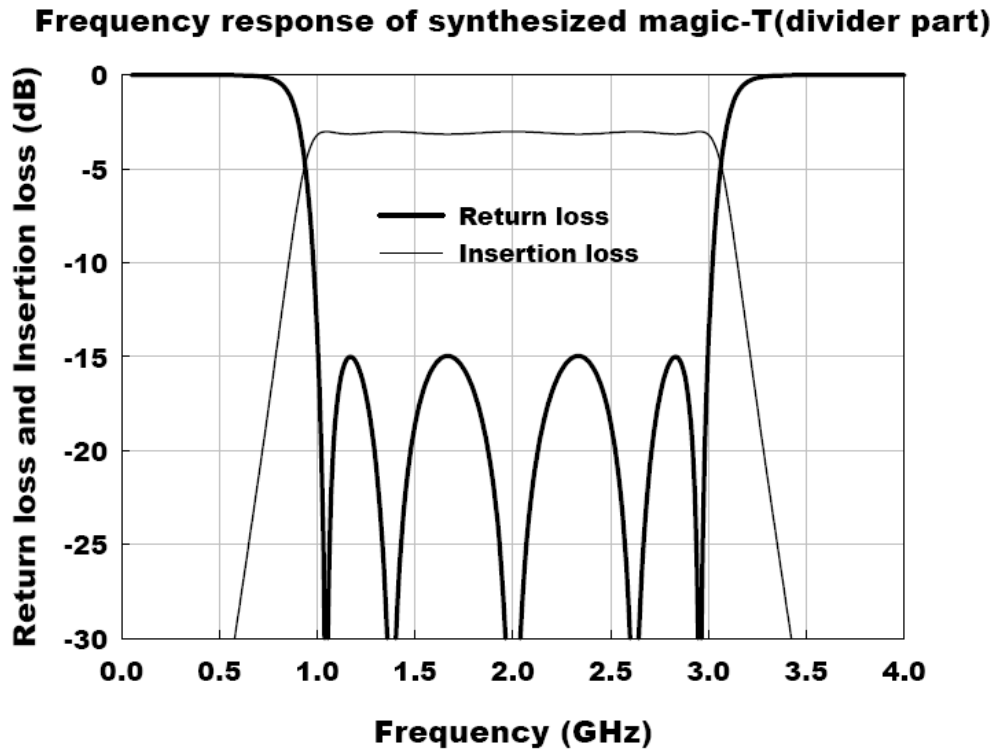


Figure 3.12 Frequency response of the synthesized power divider

### 3.4 Magic-T Transformer

From the previous analysis, we can see that by applying Kuroda's Identities in circuit simplification, we'll get unequal terminations which are  $2R\left(\frac{n'}{n}\right)^2$  and  $\frac{n''^2 R}{2}$  in the balun and divider circuit, respectively.  $R$  is the value of the output port impedance that can be arbitrarily specified by designers, and the scaling factors,  $n$ ,  $n'$ , and  $n''$  will be used to transform the terminations to match the theoretical value calculated from the synthesis procedure. Hence, an impedance-transforming magic-T can be easily designed as designers replace  $R$  with different values.

So far we've done the synthesis of balun and divider circuits. However, the design of the magic-T is not finished yet. As we mentioned before, the balun and power divider circuits share a common element  $Z_4$ . When analyzing the magic-T in both odd and even modes, we manipulate the full circuit model into balun and divider

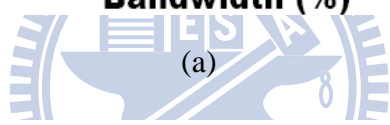
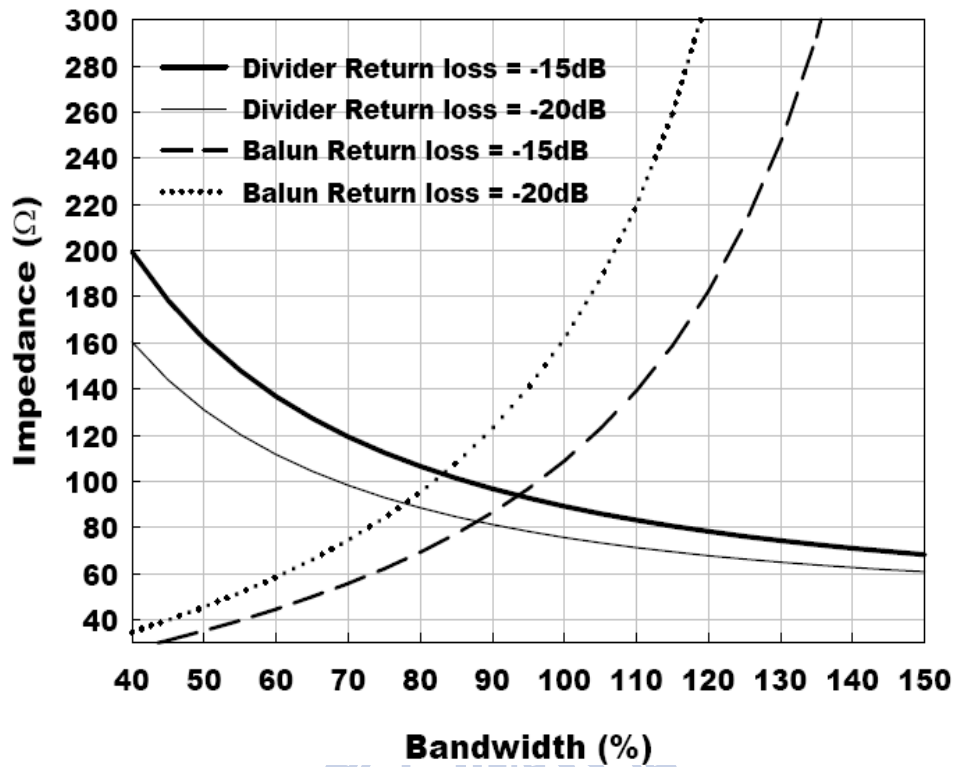
part, and then follow the synthesis procedure to find element values. Hence, we'll get two values of  $Z_4$  during the synthesis of balun and divider circuits, respectively. It's obviously not a good solution to choose the average of the two values as our final result. Instead, we should find other efficient method to determine the value of  $Z_4$  to ensure that both balun and power divider has good performance. To solve the problem of the common element, the establishment of a synthesis program is necessary.

The synthesis method we introduced previously is a systematical way that helps us construct a network. That is, we can develop a synthesis program which is more easy to use, fast, and powerful when we need to evaluate numerous cases in our design problem. With the aid of computers, we're able to rapidly find all of the element values to achieve the required response.

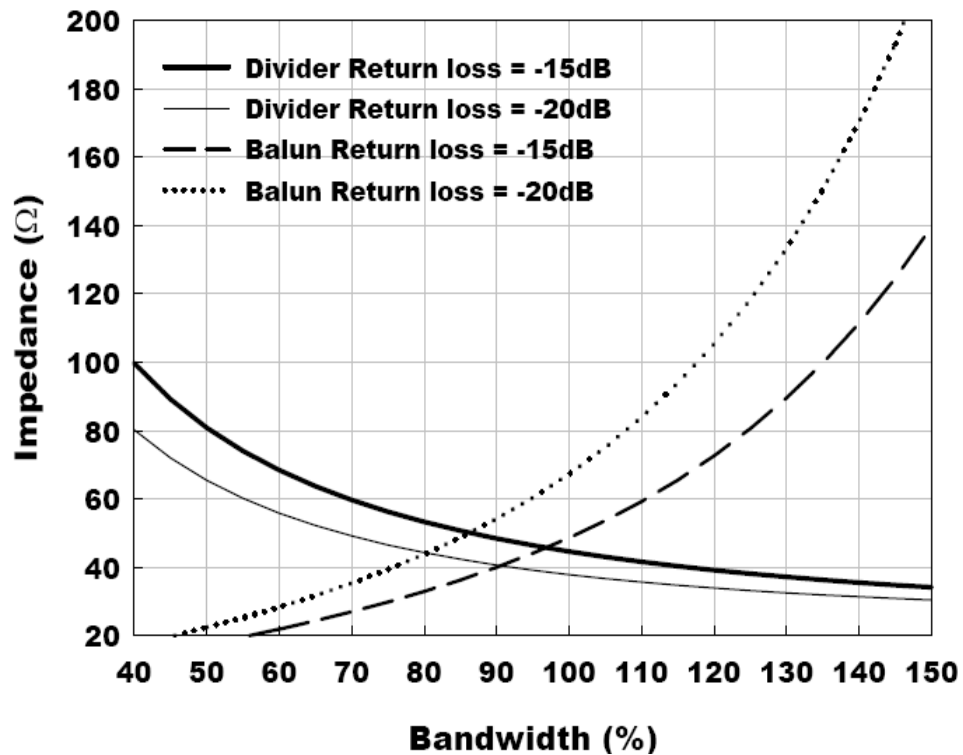
Three design graphs as shown in Figure 3.13 (a) to (c) are drawn by applying the synthesis program built for our network. The vertical axis is the value of the common element to be decided, and the horizontal axis is the bandwidth. The curves are drawn under specific return loss, which are -15dB and -20dB in our case. The figures illustrate that the impedance of the common element grows as the bandwidth increases for balun circuit. The divider circuit shows a trend that is contrary to the balun. That is, the wider the bandwidth is, the lower the impedance becomes. The intersection gives us the impedance that can be perfectly matched in both balun and divider circuits. After we determine the value of the common element, the remainder elements can directly apply the value we find during the synthesis procedure. By constructing several design graphs under user-defined specifications, we have freedom to design a magic-T which has similar or different responses in even and odd modes, respectively.

The design graphs for non 50 Ohm system as shown in Figure 3.13 (b) and (c) are also given to verify the impedance transform function of the proposed magic-T.

**Impedance of common element V.S Bandwidth(for 50Ω system)**



**Impedance of common element V.S Bandwidth(for 25Ω system)**



(b)

### Impedance of common element V.S Bandwidth(for 75Ω system)

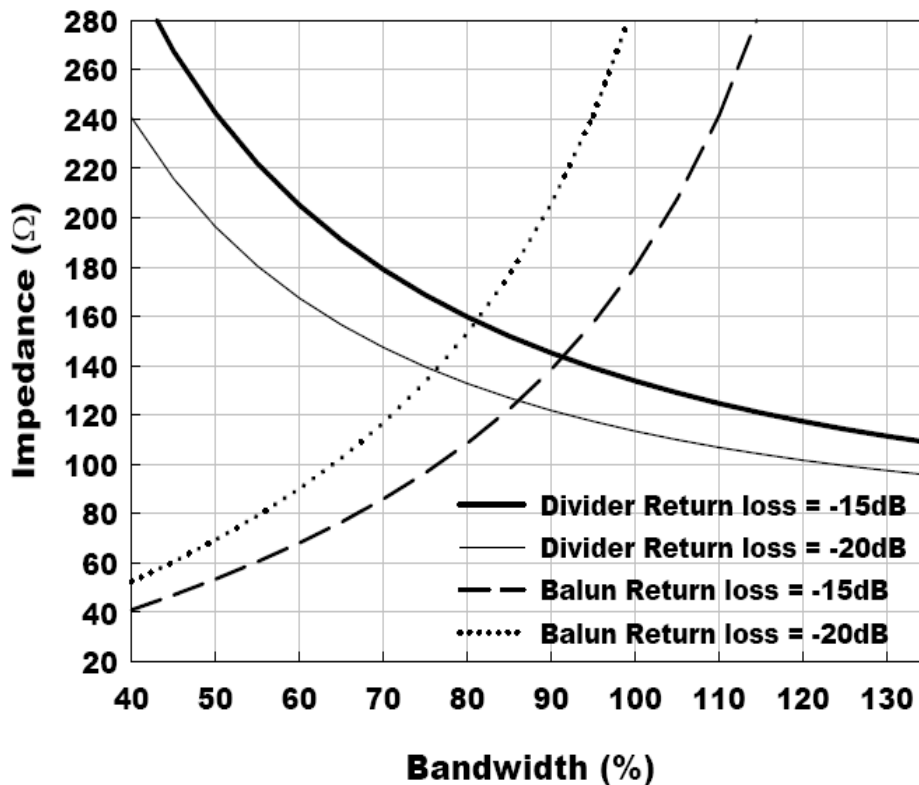


Figure 3.13 Design graph for determining the impedance of common element with specified return loss at (a)50 Ohm, (b) 25 Ohm, and (c) 75 Ohm system.

### 3.5 Simulation and Implementation

To validate the theoretical results, a broadband 180-degree hybrid is designed and implemented on RT/Duroid 6010 board with a dielectric constant of 10.2 and a thickness of 25 mil. The center frequency of the magic-T is set to be 2GHz, and is chosen to achieve 100% operating bandwidth with the return loss below -15dB for both odd and even modes. Based on the synthesis method we presented previously, each element value can be exactly determined to get the required specification. Table 3.1 lists the element value for high-pass prototype network and the original distributed network.

Table 3.1 Theoretical circuit parameters of magic-T. ( $f_o = 2GHz$ )

*Element value of magic - T*

<i>Section</i>	<i>Balun</i>		<i>Divider</i>	
<i>Specification</i>	<i>Return loss = -15dB</i> <i>BW = 100%</i>			
<i>High - pass prototype network</i> <i>(Normalized to 50Ω)</i>	$Z_1 = 1.7734$	$L' = 0.453$	$Z_4' = 3.5766$	$L'' = 0.7559$
	$Z_2' = 1.2712$	$C_1 = 0.2804$	$Z_5' = 2.5256$	$C_3 = 0.8322$
	$Z_3' = 0.9112$	load=1.6158	$C_2' = 0.1354$	load=2.0055
<i>Distributed Network</i> <i>(in 50Ω system)</i>	$Z_1 = 88\Omega$	$Z_{L1} = 108\Omega$	$Z_4 = 92\Omega$	$Z_{L3} = 68\Omega$
	$Z_2 = 149\Omega$	$Z_{L2} = 220\Omega$	$Z_5 = 65\Omega$	$Z_{L4} = 52\Omega$
	$Z_3 = 117\Omega$	$Z_{C1} = 182\Omega$	$Z_{C2} = 99\Omega$	$Z_{C3} = 59\Omega$

The schematic layout of the magic-T is demonstrated in Figure 3.14. To make the whole magic-T planar, double-layer PCB process is used to implement the magic-T. Microstriplines, slotlines, and coplanar striplines are adopted in our circuit. The analysis and characteristics of these structures are introduced in [18]-[23]. We use microstrip lines to form  $Z_1$ ,  $Z_{C1}$ ,  $Z_{C2}$ ,  $Z_{C3}$ ,  $Z_4$  and 50 Ohm de-embedded line sections.  $Z_2$ ,  $Z_{L2}$  are implemented with coplanar striplines and  $Z_{L3}$ ,  $Z_{L4}$ , and  $Z_5$  are constructed by slotlines. The remainder line sections,  $Z_{L1}$  and  $Z_3$ , are replaced with multi-section step-impedance lines and are implemented by both coplanar stripline and slotline structures. Such a substitution is to transform the impedance of  $Z_{L1}$  and  $Z_3$  to a desired level that can be realized by slotlines, which can provide a ground plane for the microstrip lines on the top layer. Besides, a defected-ground-structure (DGS) is used in our structure to increase the impedance of  $Z_{C1}$ . Since slotlines and coplanar striplines are used to implement shunt short stub, the



via-hole processing which results in extra fabrication step is not encountered. Table 3.2 gives all the physical parameters corresponding to Figure 3.15.

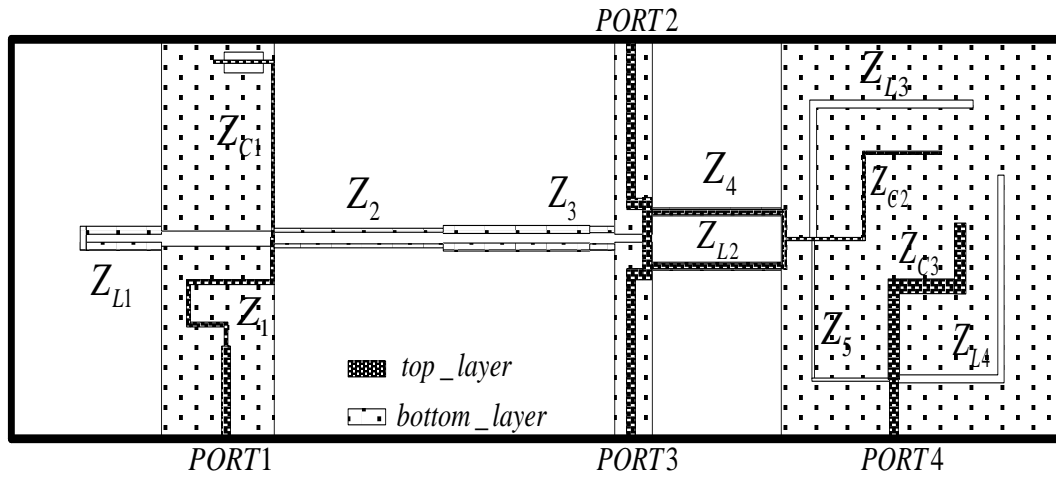
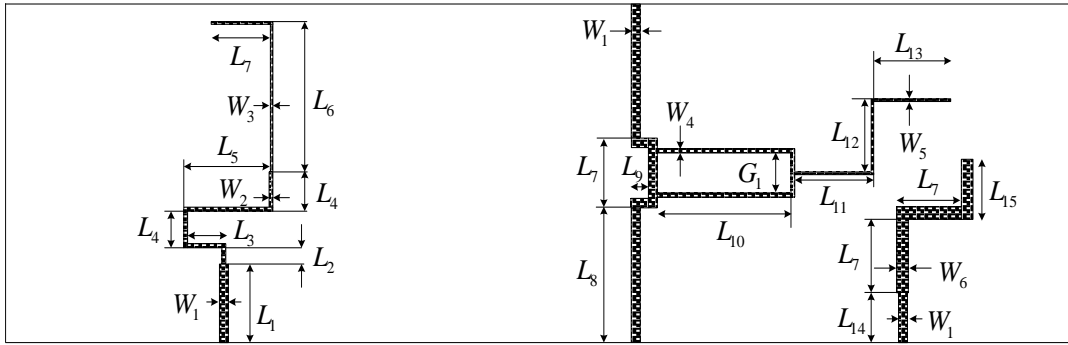


Figure 3.14 Schematic layout of the fabricated broadband magic-T.

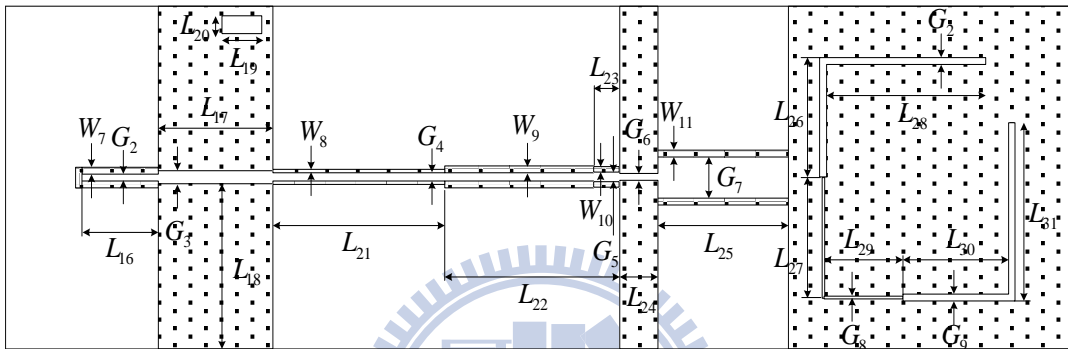
Table 3.2 The Physical dimensions of the proposed broadband magic-T corresponding to Figure 3.14. (in mil)

*Physical dimensions in mil of the magic -T  
on 25mil -thick RT / Duroid 6010 substrate*

Section	Balun	Divider
<i>Top layer</i>	$W_1 = 23$ $L_1 = 205$ $L_6 = 400$	
	$W_2 = 10$ $L_2 = 45$ $L_7 = 200$	$W_5 = 8$ $L_{11} = 217$ $L_{14} = 146$
	$W_3 = 6$ $L_3 = 155$ $L_8 = 350$	$W_6 = 28$ $L_{12} = 192$ $L_{15} = 160$
	$W_4 = 14$ $L_4 = 100$ $L_9 = 56$	$L_{13} = 240$
	$G_1 = 140$ $L_5 = 295$ $L_{10} = 520$	
<i>Bottom layer</i>	$W_7 = 20$ $G_2 = 16$ $L_{16} = 255$ $L_{21} = 640$	
	$W_8 = 13$ $G_3 = 24$ $L_{17} = 420$ $L_{22} = 495$	
	$W_9 = 18$ $G_4 = 18$ $L_{18} = 438$ $L_{23} = 85$	$G_8 = 10$ $L_{26} = 300$ $L_{29} = 270$
	$W_{10} = 15$ $G_5 = 22$ $L_{19} = 120$ $L_{24} = 116$	$G_9 = 14$ $L_{27} = 309$ $L_{30} = 307$
	$W_{11} = 16$ $G_6 = 20$ $L_{20} = 60$ $L_{25} = 500$	$L_{28} = 523$ $L_{31} = 470$
	$G_7 = 138$	



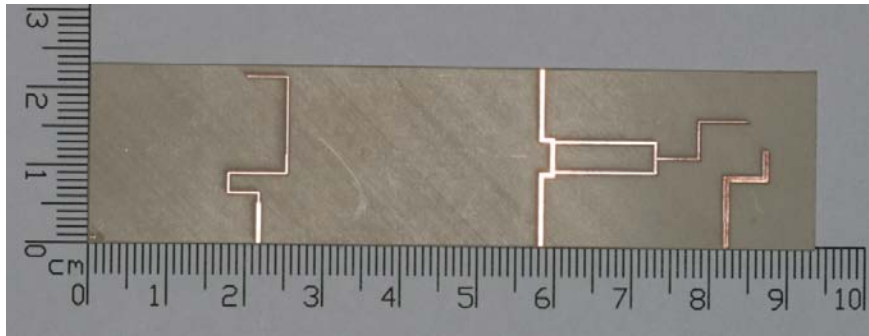
(a)



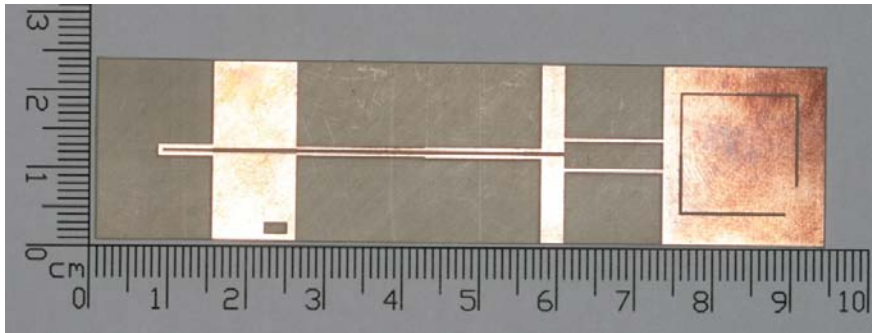
(b)

Figure 3.15 The layouts show (a) the top and (b) the bottom layer of the proposed broadband magic-T

The photographs of the fabricated magic-T including top layer and bottom layer are shown in Figure 3.16(a) and Figure 3.16(b), respectively. The circuit was measured using Agilent E5071B network analyzer. We first send power into the difference port and measure the magic-T as a balun circuit. The sum port now is terminated with a 50 Ohm broadband load. The performance of balun can be compared to the theoretical response based on HFSS simulation as shown in Figure 3.17. The measured bandwidth is slightly wider than 100% about the center frequency, 2GHz. Also the return loss is almost under -15dB in the pass band as we expected. The measured data match theoretical results well and thus verify the proposed magic-T circuit model and configuration.

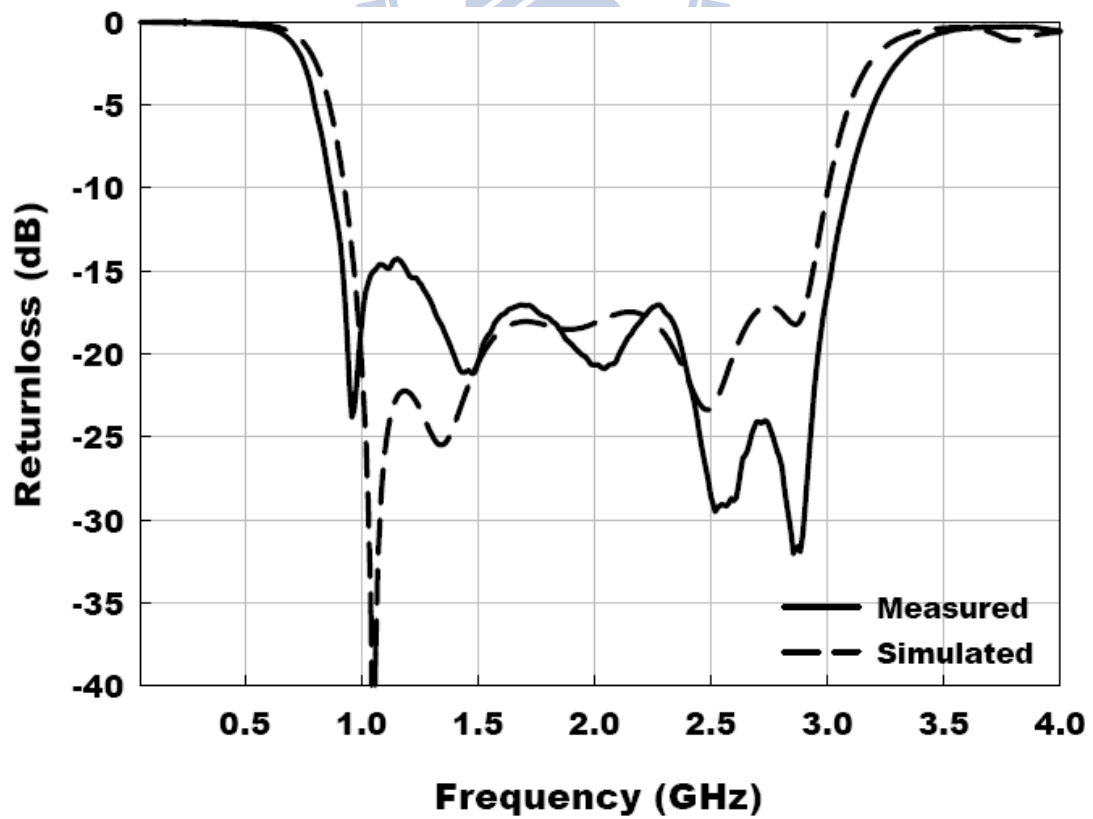


(a)

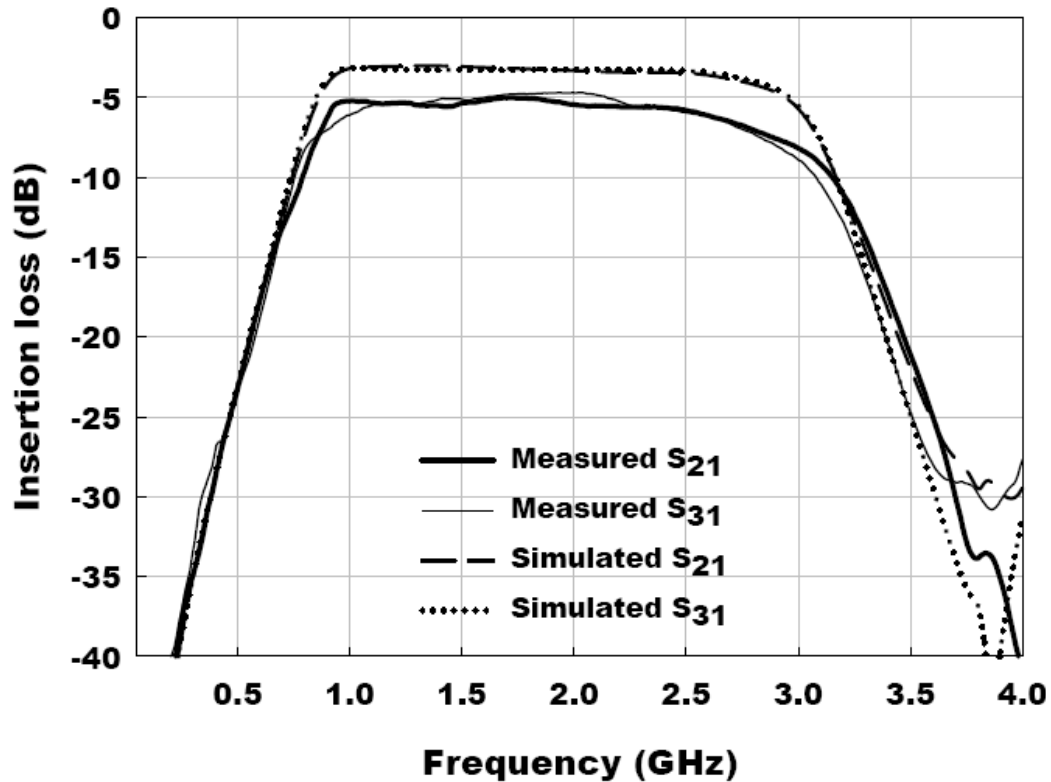


(b)

Figure 3.16 The photographs show (a) the top and (b) the bottom layer of the proposed broadband magic-T

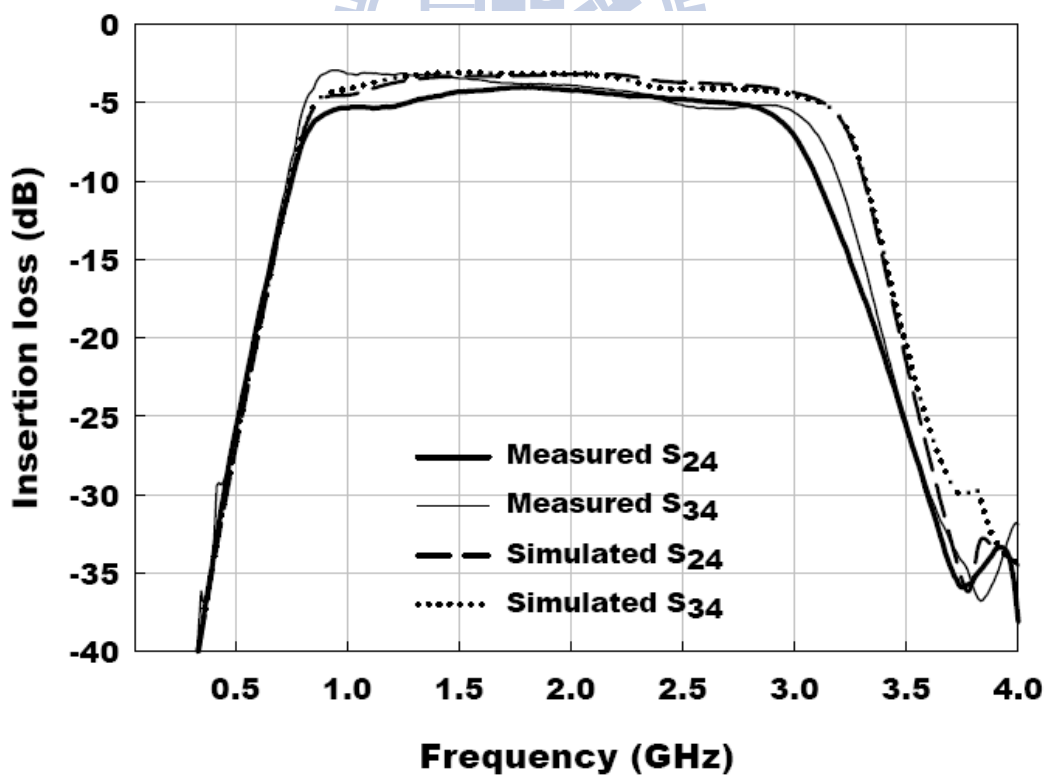
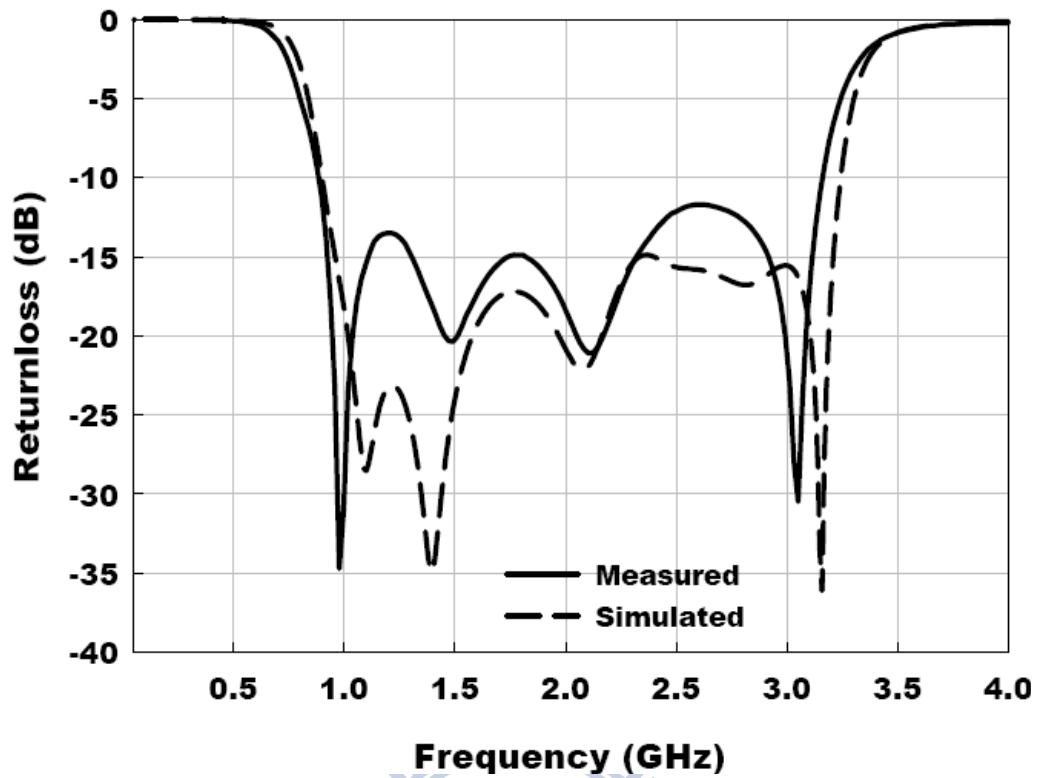


(a)



(b)  
 Figure 3.17 The simulated and measured (a) return loss and (b) insertion loss of the magic-T (in odd mode).

The performance of the divider circuit is measured by sending power into the sum port and terminating the difference port with a 50 Ohm broadband load. The simulated and measured responses are shown in Figure 3.18. We can see the divider has one more stub type element than balun and thus shows better selectivity. The bandwidth of the divider is wider than balun and the return loss is about -10 to -15dB in the pass band. The measured data have good match with the simulation results.



(b)

Figure 3.18 The simulated and measured (a) return loss and (b) insertion loss of the magic-T (in even mode).

Figure 3.19 shows that the difference port and sum port has good isolation which is measured to be lower than -30dB. The isolation between port 2 and port 3 is also given in the figure below. It exhibits similar response to the return loss of balun or divider circuits.

Both balun and divider has some insertion loss and this is due to the radiation loss caused by large area of slotlines and coplanar striplines in our magic-T. Also the increasing of the phase imbalance at high frequencies can be attributed to the asymmetry of our structure. To revise the imbalance problem we may need to use additional elements to compensate for phase variations.

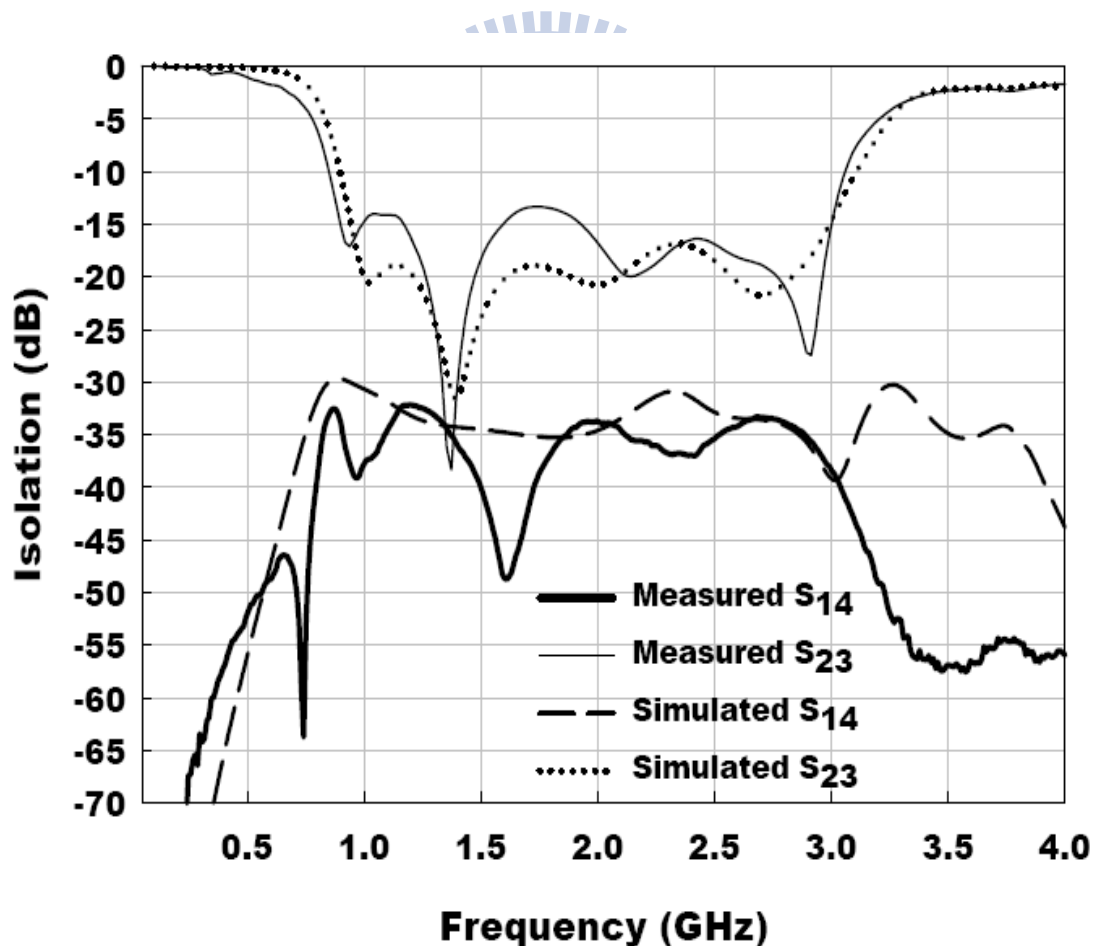


Figure 3.19 The simulated and measured isolation at port 2-3 and port 1-4 of the magic-T

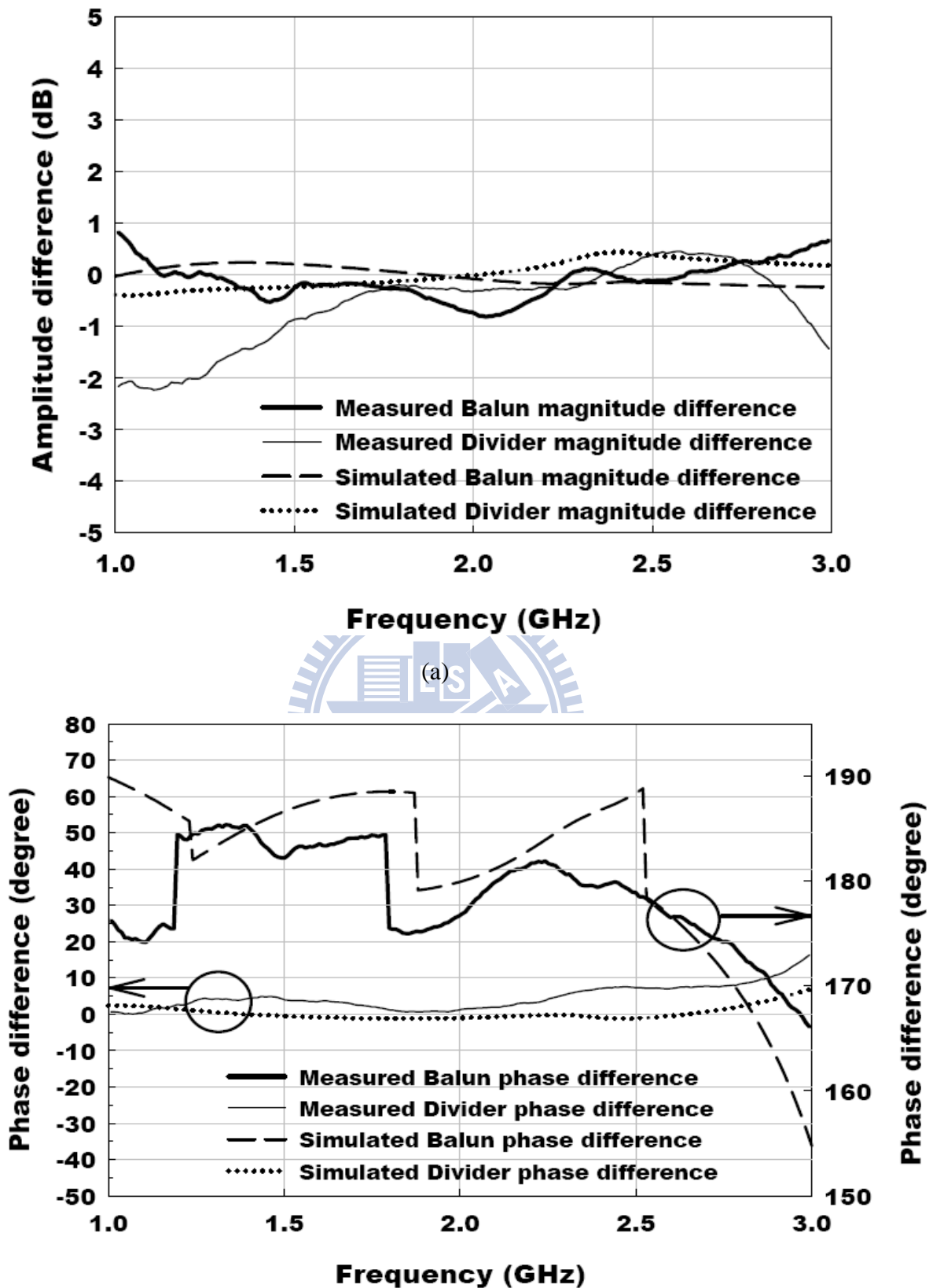


Figure 3.20 The simulated and measured (a) amplitude imbalance and (b) phase imbalance of the magic-T.





# Chapter 4

## Conclusions and Future Works

A novel broadband planar magic-T and its equivalent circuit model have been proposed. The exact synthesis method of high-pass filters with prescribed transfer functions has been applied to analyze the simplified circuit for odd mode and even mode cases, respectively. Some design graphs are also presented to give an insight into the design problem. The proposed configuration and the circuit model are validated by the result of simulation and measurement. The measured data shows that the 2GHz magic-T achieves a wide bandwidth of about 100% with 15-dB return loss, as we specified.

However, the network, consisting of a cascade of quarter-wave of transmission lines, will exhibit large size especially when it operates at low frequency. Under this condition, the use of  $S$ -plane high-pass prototype is not suitable and we must find other mapping ways to reduce the overall circuit size. Wael M. Fathelbab [24] proposed a miniaturized Marchand balun which is analyzed by  $S$ -plane band-pass prototype instead of high-pass prototype. Such a replacement permits the center frequency  $f_0$  to be different from the resonant frequency of the quarter-wave transmission line. In this case, the Richards' transformation becomes  $S = j\Omega = j \tan \frac{\pi f}{2f_q}$ , where  $f_q$  is the quarter-wave frequency of the line and will determine the size of circuit. Hence we can choose  $f_q$  to be higher than the center frequency  $f_0$  to achieve the miniaturization of the magic-T.



# References

- [1] D. Pozar, *Microwave Engineering*, 3<sup>rd</sup> edition, New York, John Wiley & Sons, 1998.
- [2] S. March, "A wide-band stripline hybrid ring," *IEEE Trans. Microwave Theory Tech.*, vol. MTT-16, p. 361, June 1968.
- [3] C. Ho, L. Fan, and K. Chang, "New uniplanar coplanar waveguide hybrid-ring couplers and magic-Ts," *IEEE Trans. Microwave Theory and Techniques*, vol. MTT-42 (1994), pp. 2440–2448.
- [4] L. Fan, S. Kanamaluru, and K. Chang, "A new wideband and reducedsize uniplanar magic-T," *IEEE MTT-S Dig Orlando, FL*, (1995), 667–670.
- [5] Chi-Yang Chang and Chu-Chen Yang, "A Novel Broad-Band Chebyshev-Response Rat-Race Ring Coupler," *IEEE Trans. Microwave Theory and Techniques*, vol. 47, no. 4, pp. 455-462, Apr. 1999.
- [6] J. P. Kim and W. S. Park, "Novel configurations of planar multilayer Magic-T using microstrip-slotline transitions," *IEEE Trans. Microwave Theory and Techniques*, vol. 50, no. 7, pp. 1683-1688, Jul. 2002.
- [7] K. U-yen, E. J. Wollack, S. Horst, T. Doiron, J. Papapolymerou, and J. Laskar, "Slotline stepped circular rings for low-loss microstrip-to-slotline transitions," *IEEE Microw. Wireless Compon. Lett.*, vol. 17, no. 2, pp. 100-102, Feb. 2006.
- [8] K. U-yen, E. J. Wollack, J. Papapolymerou, and J. Laskar, "A compact low-loss planar Magic-T using microstrip-slotline transitions," in *IEEE MTT-S Int. Microw. Symp. Dig.*, Honolulu, HI, pp. 37-40, Jun. 2007.
- [9] K. U-yen, E. J. Wollack, J. Papapolymerou, and J. Laskar, "A broadband planar Magic-T using microstrip-slotline transitions," *IEEE Trans. Microwave Theory*

- and Techniques*, vol. 56, no. 1, Jan 2008.
- [10] K. S. Ang and D. Robertson, "Analysis and design of impedance transforming planar Marchand baluns," *IEEE Microwave Theory and Techniques*, vol. 49, no. 2, pp. 402-406, Feb. 2001.
- [11] M. C. Horton and R. J. Wenzel, "General theory and design of optimum quarter-wave TEM filters," *IEEE Microwave Theory and Techniques*, vol. MTT-13, pp. 316-327, May 1965.
- [12] P. I. Richards, "General Impedance-Function Theory," *Quart. Appl. Math*, Vol. 6, pp. 21-29, 1948
- [13] Max W. Medley, *Microwave and RF Circuits: Analysis , Synthesis and Design*. Boston, Artech House.
- [14] Weinberg, L., *Network Analysis and Synthesis*, New York: McGraw-Hill, 1962.
- [15] Guillemin, E. A., *Synthesis of Passive Networks*, New York: Wiley, 1957.
- [16] Balabanian, N., *Network Synthesis*. Englewood Cliffs, N. J.: Prentice-Hall, 1958.
- [17] K. S. Ang and Y. C. Leong, "Converting balun into broadband impedance transforming  $180^\circ$  hybrid," *IEEE Microwave Theory and Techniques*, vol. 50, no. 8, pp. 1990-1995, Aug. 2002.
- [18] K. C. Gupta, R. Garg, I. Bahl, and P. Bhartia, *Microstrip Lines and Slotlines*, 2<sup>nd</sup> edition, Boston, Artech House, 1979.
- [19] S. B. Cohn, "Slot line on a dielectric substrate," *IEEE Microwave Theory and Techniques*, vol. MTT-17, pp. 768-778, Oct. 1969.
- [20] E. A. Mariani, "Slotline characteristics," *IEEE Microwave Theory and Techniques*, vol. MTT-17, pp. 1091-1096, Dec. 1969.
- [21] B. Schuppert, "Microstrip / Slotline transitions : modeling and experimental investigation," *IEEE Microwave Theory and Techniques*, vol. 36, no. 8, pp. 1272-1282, Aug. 1988.

- [22] R. Janaswamy and D. H. Schaubert, "Characteristic impedance of a wide slotline on low-permittivity substrates," *IEEE Microwave Theory and Techniques*, vol. MTT-34, no. 8, pp. 900-902, Aug. 1986.
- [23] E. A. Mariani, C. P. Heinzman, J. P. Agrios, and S. B. Cohn, "Slot line characteristics," *IEEE Microwave Theory and Techniques*, vol. MTT-17, on. 12, pp. 1091-1096, Dec. 1969.
- [24] Wael M. Fathelbab, "New Classis of Miniaturized Planar Marchand Baluns," *IEEE Trans. Microwave Theory and Techniques*, vol. 53, no. 4, pp. 1211-1220, Apr. 2005.

